
COMET: Context and Multiplicity Decomposition for Multimodal Uncertainty Estimation

Sanghyuk Chun William Yang Amaya Dharmasiri Olga Russakovsky

Princeton University

Abstract

Uncertainty estimation has been a long-standing challenge in AI models; it amounts to “knowing what you don’t know,” and metacognition is notoriously difficult even for humans (cf. the Dunning-Kruger effect). Although it is still far from solved even in simpler classification systems, tackling it in multimodal large language models (MLLMs) is becoming increasingly important. Within MLLMs, uncertainty can stem from any of the diverse sources as well as from their relationships, and further can stem from the unbounded answers in the open-ended setting. To tackle the issues, we propose CoMet, an MLLM uncertainty estimation method by decomposing uncertainty into a context-specific term and a multiplicity-specific term. The former captures ambiguity induced by the given context (e.g., task or prompt), while the latter captures how many plausible answers determined by the context remain compatible with the given input. We train a lightweight post-hoc uncertainty module to estimate these quantities, which enables efficient uncertainty estimation without autoregressive answer generation or repeated sampling. Experiments on various open-ended multimodal benchmarks, hallucination detection, and multiple-choice visual question answering benchmarks show that CoMet consistently improves uncertainty estimation over existing baselines while remaining efficient in practice. Code is available at https://github.com/princetonvisualai/comet_uncertainty

1 Introduction

Multimodal large language models (MLLMs) are increasingly used in complex and open-ended settings where inputs are diverse and outputs are not always verifiable. Consequently, reliable uncertainty estimation becomes critical for downstream decision-making: beyond solely producing an answer, a model should also assign a score that reflects the ambiguity of the prediction for a given input. This score can be used for self-evaluation (whether a prediction is correct) [1–5], abstention (whether a model can correctly answer the given input) [6–9], self-improvement [10], or hallucination detection [11, 12]. However, uncertainty estimation in MLLMs is challenging due to two fundamental properties: the diversity of uncertainty sources and the open-ended nature of the answer space.

First, uncertainty can arise from each modality as well as from their many-to-many relationship. Let us take a vision-language task as an example. Visual uncertainty can arise from low image quality [13, 14], *e.g.*, a blurry image is inherently more uncertain for a model. The text modality can also be intrinsically ambiguous when the text itself maps to multiple semantic meanings [15], *e.g.*, “What color is the mouse?” may refer either to the animal or to the computer equipment. Moreover, even when both the input image and the input text are individually certain, the many-to-many nature of the input-output correspondence (*i.e.*, their multiplicity [16]) can still introduce ambiguity [17]. For example, an image with multiple objects and a question “What is in this image?” can be mapped to multiple plausible textual descriptions. As a result, uncertainty in multimodal tasks is inherently compositional, and a faithful uncertainty estimate should distinguish different sources of ambiguity.

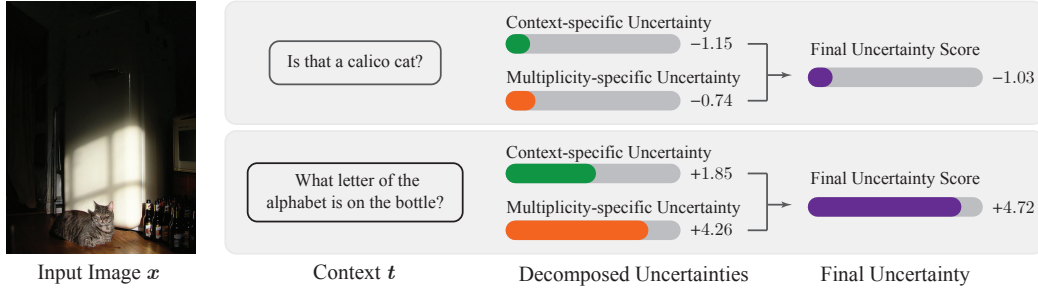


Figure 1: **Overview of the proposed multimodal uncertainty.** Even for the same image x , uncertainty could vary by the given context t . We decompose the uncertainty of a multimodal input into two components: (1) **Context-specific uncertainty** quantifies how broadly the context t defines the plausible answer space (e.g., “is that a calico cat?” induces two answers, “yes” and “no”, whereas “what letter of the alphabet is on the bottle?” induces 26 assuming the answer is in English) (2) **Multiplicity-specific uncertainty** quantifies how many context-induced plausible answers (e.g., “yes” and “no”) remain compatible with the observed input x (e.g., the cat features are visible and clearly correspond to a tabby cat, and therefore “no” is the only plausible answer, whereas the bottles are small and not well-lit, thus increasing rather than reducing uncertainty)

Second, the set of valid answers is unbounded in open-ended settings. Unlike closed-set tasks, where uncertainty can be measured over a fixed candidate set using quantities such as entropy [18] or logit confidence [19], open-ended tasks do not provide an explicit answer space to compare against. Instead, recent studies on LLM uncertainty quantification often utilize the generative capability of LLMs, for example, by asking a model to verify or verbalize its confidence [1, 3] or generating multiple answers and measuring their consistency [10]. However, these approaches rely heavily on generation performance, can inherit model-specific biases, and introduce an additional inference cost. In practice, these methods often require additional uncertainty-aware instruction tuning [20] or reinforcement learning [21] on the target LLM, which further increases training and deployment cost.

We aim to estimate the predictive uncertainty for MLLMs by considering both (1) the compositional nature of multimodal uncertainty and (2) the unbounded answer space of open-ended settings, without relying on the LLM generation capability or expensive model fine-tuning. To address these challenges, we propose a novel decomposition of predictive uncertainty into a context-specific term and a multiplicity-specific term. The first term captures the ambiguity induced by context t , where t determines the set of plausible answers. For example, in visual question answering (VQA) tasks, t is a text question. Fig. 1 shows an example: the question “What letter of the alphabet is on the bottle?” (26 plausible answers) induces a higher uncertainty than “Is that a calico cat?” (2 plausible answers). The second term captures how many plausible answers determined by context t remain compatible with the given input x . For example, the image clearly shows that the cat is a tabby cat; therefore, only “No” remains compatible when x is given.

Our decomposition is derived by introducing a new binary variable m . The matching variable m indicates whether an input x and an answer y are semantically matched under a context t (Fig. 2 illustrates their relationship more formally). For example, an image of a cat and an answer “a cat” are matched ($m = 1$) under the context “What is in this image?”. Meanwhile, for the same image and context, the answer “a dog” is not matched ($m = 0$). Using this variable, we define a match-conditioned posterior $p(y | x, t, m = 1)$ and quantify its uncertainty using entropy. However, in open-ended settings, standard discrete entropy is not directly applicable because the answer space is not explicitly enumerable and can be viewed as continuous. Therefore, we employ Rényi entropy, a generalized entropy measure, to quantify uncertainty over this posterior. In this formulation, our uncertainty is defined in terms of the matching probability $p(m = 1 | x, t, y)$ and the context-conditioned answer distribution $p(y | t)$. Therefore, by introducing matching m , we define uncertainty in terms of semantic compatibility $p(m = 1 | x, t, y)$ rather than the model-specific generation distribution $p_\theta(y | x, t)$, which may introduce a model-specific bias.

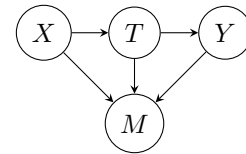


Figure 2: **The graphical model for X, Y, T and M .**

In practice, estimating uncertainty under our formulation requires two quantities: the matching probability $p(m = 1 | x, t, y)$ and the context-conditioned answer distribution $p(y | t)$. We obtain the former using an MLLM-as-verifier strategy and approximate the latter with a finite candidate-answer

set by a simple dataset construction procedure. Using these two ingredients, we train lightweight post-hoc uncertainty modules that predict our uncertainty formulation from an input x and a context t . Once trained, our uncertainty estimation module requires only x and t at inference time, without access to the candidate-answer set, any generation process, or sampling process from an MLLM.

We evaluate our uncertainty estimation framework, named **Context and Multiplicity Decomposition** (COMET) for Uncertainty estimation, on diverse open-ended multimodal benchmarks, including VQA v2 [22], VizWiz [23], and OK-VQA [24]. We additionally evaluate our method on a hallucination detection benchmark [25] and multiple choice VQA benchmarks, such as MMMU [26], MMMU Pro [27], and MMStar [28]. We validate COMET across multiple backbones, including Qwen3VL 2B, 4B, 8B Instruct [29], and InternVL3.5-1B [30]. Across these settings, COMET more reliably identifies inputs that are likely to be incorrect than existing baselines. Importantly, our method remains generation-free at inference time, making it more efficient in practice than existing methods.

Contributions. First, we introduce a new binary matching m for an input x , context t , and answer y , define a match-conditioned posterior over answers (Sec. 3.1), and quantify its uncertainty with Rényi-2 entropy (Sec. 3.2). This approach yields a novel decomposition into a *context-specific term*, which quantifies how broadly the context defines the plausible answer space, and a *multiplicity-specific term*, which quantifies how many context-plausible answers remain compatible with the observed input. Second, we develop a practical estimator for the proposed uncertainty by employing an MLLM verifier to estimate matching probabilities (Sec. 4.1), constructing an empirical approximation to $p(y | t)$ from collected candidate answers (Sec. 4.2), and training lightweight post-hoc heads to predict uncertainty from (x, t) alone (Sec. 4.3). We refer to the proposed pipeline as COMET. Third, COMET outperforms existing baselines across open-ended VQA, hallucination detection, and MCQ benchmarks, while we can take advantage of our decomposed components, *e.g.*, interpretable information about different sources of ambiguity (Sec. 5.3).

2 Related Work

Sampling-based uncertainty for M/LLM. Sampling-based methods estimate uncertainty by aggregating multiple outputs, *e.g.*, quantify the output consistency [10] or their semantic meaning [12, 31]. In MLLM, the diverse outputs can also be generated by perturbing input pixels [11]. While these methods can estimate meaningful uncertainty quantities, they require multiple generations, which limits their practicality. We estimate uncertainty efficiently without generation.

M/LLM-as-uncertainty estimator. Instead of generating samples repeatedly, a line of study attempts to let an LLM directly quantify its uncertainty. For example, Kadavath et al. [1] derives uncertainty by the probability of the “True” token when a user asks whether the generated output is correct. As another example, Tian et al. [3] lets a model predict its uncertainty in a verbalized form, *e.g.*, “confidence is 8/10”, along with its generated output. These methods empirically show their effectiveness, but they remain tied to model-specific confidence proxies or generation behavior. On the other hand, our decomposed uncertainty formulation reduces the reliance on the model capability.

In Appendix A, we provide a more comprehensive discussion, including methods that require expensive fine-tuning and methods that decompose uncertainty. In summary, COMET enables efficient uncertainty estimation inference using a lightweight post-hoc module, and our decomposition provides a theoretically motivated perspective that differs from existing uncertainty decompositions.

3 Context and Multiplicity Decomposition for Uncertainty Estimation

In this section, we introduce a novel decomposition of multimodal uncertainty into context-specific and multiplicity-specific terms. Our key idea is to introduce a binary variable, matching m , which indicates whether an input x and an answer y are semantically compatible under a context t . We then derive a match-conditioned posterior and quantify its uncertainty using Rényi entropy. Our formulation has two advantages: it provides a theoretically motivated uncertainty decomposition, and it can be applied to open-ended settings where the answers cannot be explicitly enumerated.

3.1 Matching probability to posterior

Let X denote the input, Y the output, and T the context that specifies the space of Y , such as a task description or a text prompt. X , Y and T can be continuous. In this paper, we assume the simplest scenario, where X is an image, T is a text question or instruction, and Y is the generated answer.

A natural starting point for uncertainty estimation is the predictive distribution $p(y | x, t)$, whose uncertainty quantifies how uncertain the output y is under given input x and context t . However, directly using this objective can be problematic in open-ended settings. First, the output space may be large or unbounded, making direct uncertainty estimation computationally expensive and often dependent on heavy sampling. Second, in practice, we approximate the distribution $p(y | x, t)$ using a pre-trained MLLM p_θ , which may have a model-specific bias. We therefore reformulate the problem on the basis of semantic validity rather than raw generation by models. To achieve this, we introduce a binary variable $M \in \{0, 1\}$ that indicates whether x and y are matched under the given t .

We introduce a probabilistic graphical model to capture the relationship between X , T , Y and M in Fig. 2. First, a context T defines a prior over outputs Y . For example, if a task is classification, then the possible outputs are determined by the desired class names. We also assume that a context T is defined when we have an input X . For example, assume that we have an image with numbers. In this case, we can imagine different tasks about the image, *e.g.*, ‘‘What is the summation of the numbers?’’ or ‘‘What is the largest number?’’. Finally, we assume that M is determined if all X , T , and Y are given. Namely, we cannot confirm if X and Y are matched without knowing what the context T is.

In this setting, we can derive the posterior of Y for the given x and t when they matched ($m = 1$), $\pi_y := p(y | x, t, m = 1)$, using Fig. 2 and the matching probability $p(m = 1 | x, t, y)$ as follows:

$$\pi_y = \frac{p(m = 1 | x, t, y)p(y | x, t)}{\int p(m = 1 | x, t, y')p(y' | x, t)dy'} \stackrel{\text{(by Fig. 2)}}{=} \frac{p(m = 1 | x, t, y)p(y | t)}{\int p(m = 1 | x, t, y')p(y' | t)dy'}. \quad (1)$$

There are several advantages of introducing $p(m = 1 | x, t, y)$. First, our formulation removes the direct dependence on the predictive distribution $p(y | x, t)$. In practice, an estimated generative distribution $p_\theta(y | x, t)$ may suffer from decoder bias, paraphrase variation, or any other model-specific bias; therefore, it may not faithfully capture the semantic ambiguity of the posterior. On the other hand, by employing a binary random variable M , we instead reformulate the problem in terms of semantic compatibility between the input and a candidate answer. Second, our formulation naturally extends from a finite discrete answer space to an open-ended one. In discrete settings, matching can be viewed as indicating whether each candidate answer is valid under the given input and context. By relaxing this notion to be a soft matching probability, our formulation can be applied even when the answer space is not explicitly enumerable.

3.2 Uncertainty Decomposition

Our goal is to estimate the uncertainty of the match-conditioned posterior, Eq. (1). If Y is discrete and its distribution is explicitly given (*i.e.*, in closed-set settings), we can easily compute its information entropy by $\mathbb{E}_{Y \sim \pi_y}[-\log \pi_Y]$. However, in open-ended settings, the underlying distribution of Y is unknown and can even be continuous, and discrete entropy is not applicable.

To mitigate this problem, we use a generalized notion of entropy, specifically Rényi-2 entropy, defined by $H_2(p(x)) := -\log \int_x p(x)^2 dx$. Rényi entropy is a generalized version of entropy, which is defined by $H_\alpha(p(x)) := \lim_{\gamma \rightarrow \alpha} \frac{1}{1-\gamma} \log \int p(x)^\gamma dx$; if $\alpha = 1$, it is the same as Shannon’s entropy in discrete cases and differential entropy in continuous cases. The case of $\alpha = 2$, also known as collision entropy or Simpson diversity index, is particularly suitable in our case because it quantifies how concentrated the distribution is. We provide a more detailed discussion in Appendix B.1.

Let $Z_1(x, t) := \mathbb{E}_{Y \sim p(\cdot|t)}[p(m = 1 | x, t, Y)]$ and $Z_2(x, t) := \mathbb{E}_{Y \sim p(\cdot|t)}[p(m = 1 | x, t, Y)^2]$. We assume that $p(y | t)$ is a uniform distribution over a restricted region Ω , *i.e.*, $p(y | t) = \frac{1}{\int_\Omega dy} := \frac{1}{K_t}$. Then the Rényi-2 entropy of Eq. (1) can be computed as follows:

$$\begin{aligned} u(x, t) &:= -\log \int \pi_y^2 dy = -\log \int \frac{p(m = 1 | x, t, y)^2 p(y | t)^2}{Z_1(x, t)^2} dy = -\log \left[\frac{1}{K_t} \frac{Z_2(x, t)}{Z_1(x, t)^2} \right] \\ &= \underbrace{\log K_t}_{:=u_t(t)} + \underbrace{2 \log Z_1(x, t) - \log Z_2(x, t)}_{:=u_{x|t}(x|t)}, \end{aligned} \quad (2)$$

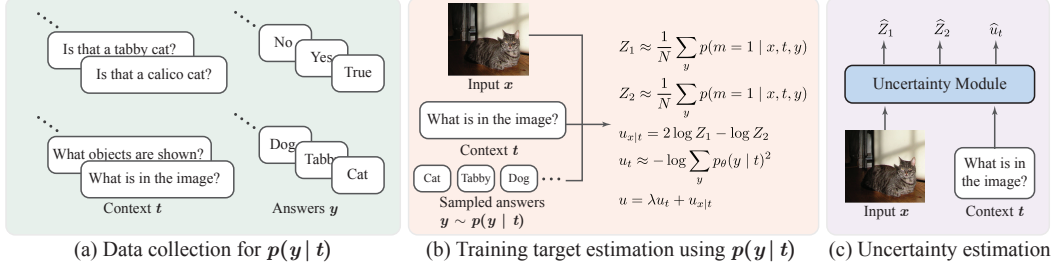


Figure 3: **Overview of the proposed COMET framework.** (a) We construct a context-conditioned answer distribution $p(y | t)$ based on text clustering on the Cambrian dataset [32] (Sec. 4.2). (b) Using the MLLM-based matching probability estimator (Sec. 4.1), we estimate the uncertainty targets from the constructed dataset. (c) We train a light-weight uncertainty module using the constructed dataset and the estimated targets (Sec. 4.3).

where the more detailed derivation is in Appendix B.2. In Eq. (2), the uncertainty is decomposed by (1) the context-specific term $u_t(t)$ and (2) the multiplicity-specific term $u_{x|t}(x | t)$. More specifically, $u_t(t)$ captures how broad the plausible answer space for the given context $p(y | t)$ is:

$$u_t(t) = \log K_t = -\log p(y | t) \underset{(\text{if } p(y | t) \text{ is uniform})}{=} -\log \mathbb{E}_{Y \sim p(\cdot | t)}[p(y | t)] = H_2(p(y | t)). \quad (3)$$

In other words, if the context t is ambiguous to answer, we naturally have a high uncertainty. For example, the context “describe this image” (K_t is almost infinitely large) has a higher uncertainty than the context “Is there a cat in this image? Answer yes or no” (K_t is 2).

When we take a look into the multiplicity-specific term $u_{x|t}(x | t)$, we have the following relationship:

$$u_{x|t}(x | t) = 2 \log Z_1(x, t) - \log Z_2(x, t) = -\log \left(\frac{\text{Var}_{Y \sim p(\cdot | t)}[p(m = 1 | x, t, Y)]}{\{\mathbb{E}_{Y \sim p(\cdot | t)}[p(m = 1 | x, t, Y)]\}^2} + 1 \right), \quad (4)$$

which implies that $u_{x|t}(x | t)$ can be represented in a form related to coefficient of variation (or relative standard deviation) of the matching probability over the distribution $p(y | t)$. In other words, if the matching probabilities $p(m = 1 | x, t, y)$ are very similar for all the possible y (i.e., how many y can be matched to x with the given t), then we have a high uncertainty value. We provide a more detailed discussion related to u_t and $u_{x|t}$ in Appendix B.2. We also show that we can have a similar formulation with Eq. (2) even with discrete entropy. Details are provided in Appendix B.3.

4 Practical Uncertainty Estimation

In practice, estimating uncertainty under our formulation in Eq. (2) requires two quantities: the matching probability $p(m = 1 | x, t, y)$ and the context-conditioned answer distribution $p(y | t)$. For the matching probability, we adopt an MLLM-as-verifier strategy. Estimating $p(y | t)$ is more challenging. We construct a candidate-answer set that approximates $p(y | t)$, which is less model-dependent and more efficient than employing generative models. Using these two ingredients, we train lightweight post-hoc uncertainty modules that predict our uncertainty formulation from an input x and a context t . Once the module is trained, the uncertainty can be estimated from x and t alone without requiring any generation process or sampling process from an MLLM, which makes the overall inference efficient. The overview of our framework COMET is illustrated in Fig. 3.

4.1 Verification as matching probability

Our decomposition requires a matching probability function $p(m = 1 | x, t, y)$. We can employ a parameterized matching probability module, which is a binary classifier that takes a (x, t, y) triplet as input. However, we found that training a reliable matching probability module is difficult and does not generalize well to arbitrary open-ended settings. More detailed discussions are in Appendix C.1.

Instead of training a separate matching probability module, we employ an MLLM as a verifier of matching. For example, we let an MLLM take “Image:{x}, Question:{t}, Proposed Answer:{y}. Is this answer correct? Answer Yes or No.”, then compute the probability of “Yes” (the full prompt can be found in Appendix C.2). This simple technique is known to be

effective in estimating self-correctness despite its simplicity [1]. We additionally employ affine transform parameters (β, γ) to calibrate the matching probability as follows:

$$p(m = 1 | x, t, y) = \text{sigmoid} \left(\beta \log \frac{p(\text{“Yes”} | x, t, y)}{p(\text{“No”} | x, t, y)} + \gamma \right), \quad (5)$$

If $\beta = 1, \gamma = 0$, Eq. (5) becomes $p(\text{“Yes”} | x, t, y) / (p(\text{“Yes”} | x, t, y) + p(\text{“No”} | x, t, y))$. In our experiments, we calibrate β and γ from a validation dataset. See more details in Appendix C.3.

4.2 Approximating the context-conditioned answer distribution

We also require $p(y | t)$ to our uncertainty estimates. One possible approach is to approximate it using a language model, *i.e.*, $p(y | t) \approx p_\theta(y | t)$. However, this can introduce model-specific bias and is computationally expensive. Instead, we construct a candidate-answer set that approximates $p(y | t)$, which is less model dependent and more efficient.

Instead of relying on generative models, we collect plausible answers from a visual instruction tuning dataset, which consists of image-prompt-answer triplets. We first collect all prompt texts and their corresponding answers from the Cambrian dataset [32]. Then, we perform a simple greedy clustering on the prompts. After clustering, we treat all the answers from the same cluster as the plausible answers of the questions in the cluster. For example, assume that we have a question “what is in this image?” and its answer “a cat”, and another question-answer pair “what is in this photo?” and “a bird” in a cluster. In this case, both “a cat” and “a bird” are treated as plausible answers of the question “what is in this image?”. We describe the details of the collection procedure in Appendix C.4.

4.3 Training objective

Now, we approximate the quantities Z_1, Z_2 (Eq. (4)), u_t (Eq. (3)), and u (Eq. (2)) defined in Sec. 3.2 using the matching probability $p(m = 1 | x, t, y)$ in Sec. 4.1 and the context-conditioned answer distribution $p(y | t)$ in Sec. 4.2.

First, given a finite candidate-answer set \mathcal{Y}_t that approximates $p(y | t)$, we can approximate $u_{x|t} = 2 \log Z_1(x, t) - \log Z_2(x, t)$ as follows:

$$\widehat{Z}_1(x, t) = \frac{1}{|\mathcal{Y}_t|} \sum_{y' \in \mathcal{Y}_t} p(m = 1 | x, t, y') \quad \widehat{Z}_2(x, t) = \frac{1}{|\mathcal{Y}_t|} \sum_{y' \in \mathcal{Y}_t} p(m = 1 | x, t, y')^2. \quad (6)$$

Estimating $u_t(t)$ is more challenging because we cannot access the true $p(y | t) = \frac{1}{K_t}$ distribution, hence K_t is unknown. Instead, we employ a practical approximation using a tractable density estimator $p_\theta(y | t)$, *i.e.*, an autoregressive LM, based on Eq. (3) as follows:

$$u_t(t) = H_2(p(y | t)) \approx \widehat{u}_t(t) = -\log \sum_{y' \in \mathcal{Y}_t} p_\theta(y' | t)^2, \quad (7)$$

where $p_\theta(y' | t)$ can be computed using the autoregressive nature of LMs. Since this surrogate breaks the uniform assumption of $p(y | t)$, Eq. (7) is not exactly the same as the original $u_t(t)$. To control the effect of the approximation error, we add a control hyperparameter λ as follows:

$$\widehat{u}(x, t) = \lambda \widehat{u}_t(t) + 2 \log \widehat{Z}_1(x, t) - \log \widehat{Z}_2(x, t). \quad (8)$$

Using the collected data samples described in Sec. 4.2, we optimize a light-weight head that estimates $\widehat{Z}_1(x, t), \widehat{Z}_2(x, t)$ and $\widehat{u}_t(t)$ using a regression loss. After training the module, we additionally employ a light-weight adaptation process on a small number of data samples related to the target benchmark. More details of the model architecture and the objective functions are in Appendix C.5.

5 Experiments

In this section, we evaluate CoMET for its capability to improve MLLM uncertainty estimation. We first evaluate CoMET on open-ended multimodal understanding, unanswerability/hallucination detection, and multiple-choice question (MCQ) settings (Sec. 5.2). Next, we examine the effectiveness of our proposed decomposition formulation by quantitative and qualitative studies (Sec. 5.3).

5.1 Experimental setup

Benchmarks. We evaluate COMET on open-ended VQA benchmarks, including VQA v2 [22], VizWiz [23], and OK-VQA [24]. For VQA v2, we randomly subsample 10k samples from the dataset to reduce the inference cost of sampling or generation-based methods (the original VQA v2 consists of 214k samples). We additionally consider two complementary reliability tasks: unanswerability detection on VizWiz and hallucination detection on HallusionBench [25]. Finally, we evaluate COMET on MCQ VQA benchmarks, including MMMU (test split) [26], MMMU Pro [27], and MMStar [28]. We describe more details of each benchmark in Appendix D.1.

Evaluation metrics. We report standard uncertainty estimation metrics, such as AUROC, AUPR, and FPR95. Following common practice, we treat uncertainty estimation as a binary classification problem where the uncertainty score is used to distinguish correct predictions from incorrect ones. For open-ended VQA whose evaluation is based on a soft VQA score, we use a threshold to make the prediction binary. We describe the details of our evaluation metrics in Appendix D.2.

Implementation details. Using the data collection process described in Sec. 4.2, we collect 200,000 image-question pairs, where each pair is associated with 32 plausible answers. We split this dataset into 199k training samples and 1k validation samples. Model selection is performed on the 1k validation split, and the hyperparameter search is performed on the MMMU validation split (900 samples). In our hyperparameter study, we set $\beta = 0.2$ and $\gamma = -0.1$ for Eq. (5) across all backbones. For Eq. (8), we use $\lambda = 0.25$ for all backbones except Qwen3VL-4B-Instruct, for which $\lambda = 1.0$ performs best. For adaptation, we use 900 samples of the MMMU validation split [26] and 10k randomly selected samples from VQA v2 [22], not overlapped with our selected 10k test split.

We evaluate four MLLM backbones: Qwen3VL-2B-Instruct, Qwen3VL-4B-Instruct, Qwen3VL-8B-Instruct [29], and InternVL3.5-1B [30]. For each backbone, we use the selected backbone for matching probability estimator (Eq. (5)), and train a separate uncertainty module while keeping the original MLLM weight fixed. The full implementation details are provided in Appendix D.3.

Comparison methods. We compare COMET against four groups of methods. (1) *Generation-based* that generate an answer y for a given input x and context t , and then estimate confidence from the generated output. **Negative log-likelihood (NLL)** measures the likelihood of the generated answer under $p(y | x, t)$, **P(Correct)** [1] estimates confidence from the token probability of “Yes” when the model is asked a follow-up question, *e.g.*, “Is this answer correct?”. **Verbalized confidence** [3] asks the model to produce its confidence in text, *e.g.*, “confidence is 6/10”. (2) *Sampling-based* that generate multiple answers for the same input and estimate uncertainty from their consistency. We consider **consistency entropy** and **consistency maximum probability**, both computed from the empirical answer distribution induced by repeated sampling [10]. (3) *Perturbation-based*: we compare against **VL-Uncertainty** [11], which derives MLLM uncertainty from consistency of generated outputs with perturbed images. (4) *Candidate-based baselines*: for MCQ VQA, we additionally report **candidate entropy** and **candidate maximum probability**, computed over the explicit answer options. More details of the methods are provided in Appendix D.4.

5.2 Main results

Open-ended VQA. We first evaluate COMET on open-ended VQA benchmarks, including VQA v2, VizWiz, and OK-VQA. The first part of Tab. 1 and Tab. E.1 show that COMET consistently outperforms existing baselines across all three benchmarks and all backbones. For example, on the Qwen3VL-2B backbone, COMET improves the average score by +0.100 AUROC over the strongest baseline, P(Correct). Importantly, COMET is generation-free at inference time, yet substantially outperforms MLLM-specific uncertainty estimation methods requiring repeated generation, *e.g.*, VL Uncertainty [11], with a large gap (*e.g.*, +0.135 average AUROC).

Error detection. We next evaluate whether the proposed uncertainty estimates transfer to related reliability tasks, such as unanswerability detection on VizWiz and hallucination detection on HallusionBench. They are complementary to open-ended VQA because they require uncertainty estimates to identify predictions that are unsupported or unreliable, rather than rank answer confidence. As shown in the second part of Tab. 1, COMET achieves the best average performance across all backbones. The full results in Tab. E.2 show that COMET achieves either the best or second-best performance on all sub-benchmarks. This supports that our decomposed uncertainty formulation can be extended to a more general uncertainty use cases.

Table 1: **Main comparison results.** We report AUROC (AUC), AUPRC (AP), and FPR@95 of uncertainty estimation methods on three settings: open-ended multimodal understanding, error detection, and MCQ VQA. We report the average score for each setting; the full results are in Appendix E.1. “GF” denotes generation-free.

		Qwen3VL-2B-Instruct			Qwen3VL-4B-Instruct			Qwen3VL-8B-Instruct			InternVL3.5-1B		
		AUC ↑	AP ↑	FPR ↓	AUC ↑	AP ↑	FPR ↓	AUC ↑	AP ↑	FPR ↓	AUC ↑	AP ↑	FPR ↓
Open-ended multimodal understanding benchmarks (Average)													
Consist. (Ent) [10]	✗	.624	.593	.918	.661	.464	.899	.657	.548	.904	.495	.411	.959
Consist. (Max) [10]	✗	.623	.593	.914	.660	.464	.899	.655	.547	.904	.495	.411	.959
NLL	✗	.569	.545	.963	.491	.357	.974	.475	.417	.970	.576	.433	.949
Verbalized Conf [3]	✗	.591	.592	.842	.562	.378	.896	.642	.598	.787	.639	.546	.840
P(Correct) [1]	✗	.685	.648	.863	.712	.536	.837	.714	.652	.766	.667	.532	.897
VL Uncertainty [11]	✗	.650	.646	.852	.654	.605	.829	.654	.665	.829	.637	.535	.869
CoMET (Ours)	✓	.785	.784	.707	.784	.631	.717	.799	.728	.701	.734	.647	.771
Unanswerability/hallucination detection benchmarks (Average)													
Consist. (Ent)	✗	.586	.519	.886	.599	.438	.877	.614	.442	.886	.493	.441	.926
Consist. (Max)	✗	.584	.519	.892	.598	.434	.904	.610	.441	.886	.493	.441	.926
NLL	✗	.506	.465	.961	.547	.377	.943	.499	.353	.962	.514	.432	.950
Verbalized Conf	✗	.599	.567	.953	.548	.397	.930	.612	.503	.911	.615	.560	.954
P(Correct)	✗	.672	.619	.817	.648	.474	.800	.635	.467	.844	.649	.553	.812
VL Uncertainty	✗	.534	.584	.955	.522	.380	.979	.522	.376	.975	.561	.526	.884
CoMET (Ours)	✓	.751	.693	.710	.705	.540	.761	.701	.572	.765	.732	.649	.767
Multiple choice question (MCQ) visual question answering (VQA) benchmarks (Average)													
Candidate (Ent)	✓	.719	.801	.799	.680	.676	.861	.675	.646	.846	.583	.657	.921
Candidate (Max)	✓	.708	.793	.812	.673	.664	.880	.669	.635	.867	.575	.651	.928
Consist. (Ent)	✗	.775	.899	.562	.709	.813	.638	.714	.791	.658	.680	.804	.767
Consist. (Max)	✗	.766	.893	.586	.706	.807	.678	.709	.781	.688	.674	.798	.781
NLL	✗	.191	.556	.996	.247	.446	.996	.301	.452	.980	.357	.558	.994
Verbalized Conf	✗	.617	.773	.933	.540	.676	.911	.560	.640	.899	.531	.695	.892
P(Correct)	✗	.511	.688	.970	.729	.776	.763	.733	.771	.724	.589	.716	.911
VL Uncertainty	✗	.802	.909	.482	.721	.812	.660	.722	.789	.687	.587	.715	.902
CoMET (Ours)	✓	.842	.929	.438	.782	.843	.655	.783	.825	.654	.660	.772	.851

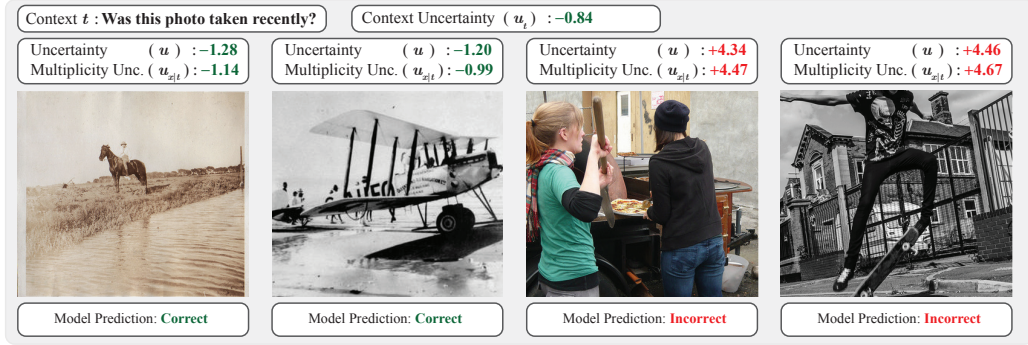
Table 2: **Impact of the proposed CoMET uncertainty decomposition.** We compare CoMET trained with various combinations of uncertainty components in AUROC scores on each benchmark. Qwen3VL-8B-Instruct is used for the backbone, and the MMMU validation split is used for the actual hyperparameter selection.

u_t	$u_{x t}$	MMMU val	VQA v2	VizWiz	OK-VQA	MMMU Test	MMMU Pro	MMStar	Avg
✓	✗	.751	.691	.691	.625	.716	.649	.677	.686
✗	✓	.837	.834	.734	.735	.753	.707	.857	.780
✓	✓	.842	.836	.815	.746	.770	.726	.853	.798

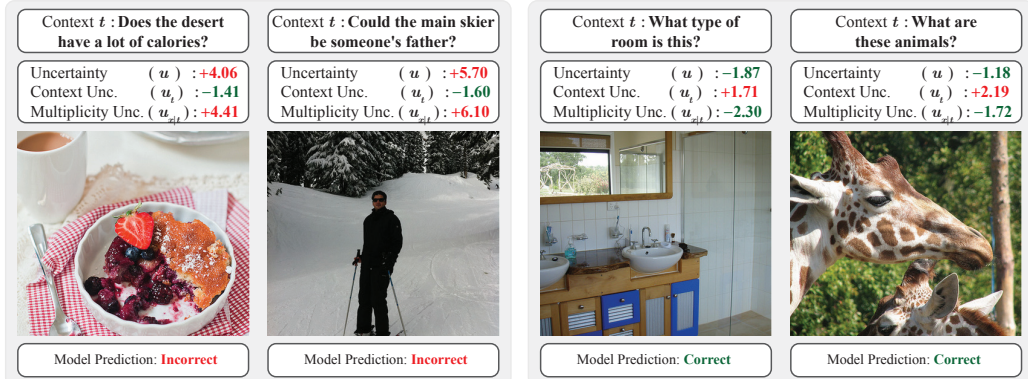
MCQ VQA. Finally, we evaluate CoMET on MCQ VQAs, including MMMU, MMMU Pro, and MMStar. Although our formulation is designed for open-ended settings rather than closed-set MCQ tasks, Tab. 1 and Tab. E.3 show that CoMET remains highly competitive in this structured setting. In most cases, CoMET outperforms the comparison methods; for some cases, such as InternVL3.5-1B, CoMET achieves the second-best performance after consistency-based baselines. We presume that this is because MCQ benchmarks provide an explicit candidate set, making repeated sampling particularly effective for estimating answer instability by reducing the search space. Nevertheless, CoMET remains competitive without repeated answer generation, suggesting that the proposed decomposed uncertainty captures semantic ambiguity that transfers beyond open-ended settings.

5.3 Analysis

Parameter study. We ablate the two components of CoMET (*i.e.*, u_t and $u_{x|t}$) in Tab. 2. Training a model with only u_t or $u_{x|t}$ performs consistently worse than using both components, *e.g.*, 0.798 average AUROC with both terms vs. 0.780 or 0.686 with each term alone. This shows that the two terms capture complementary uncertainty signals. In particular, u_t can be effective when dataset-level context priors are informative, while $u_{x|t}$ becomes important when the visual input is necessary to



(a) Samples with the same context but different images. Sorted by its uncertainty (right is more uncertain)



(b) Samples with low context unc. but high multiplicity unc. (c) Samples with high context unc. but low multiplicity unc.

Figure 4: Visualization of uncertainties of various samples.

resolve the ambiguity (e.g., VQA v2 [22]). These results support our decomposition of multimodal uncertainty into context-induced ambiguity and input-answer multiplicity.

Visualization of uncertain samples. Fig. 4 visualizes examples with the estimated uncertainty u and its decomposed components u_t and $u_{x|t}$. Fig. 4 (a) shows that the uncertainty can vary through $u_{x|t}$ even when the context t is fixed; Fig. 1 shows the complementary case where the image is fixed but the context changes. Since the question is a yes/no question, it yields low u_t . However, when the image does not provide enough visual evidence to determine “when the photo was taken”, $u_{x|t}$ becomes high, as shown in the rightmost examples. Fig. 4(b) and (c) show cases where u_t and $u_{x|t}$ behave differently. For example, the question “What are these animals?” induces a broad answer space, but the image clearly identifies the animals as giraffes, resulting in high u_t but low $u_{x|t}$.

We additionally provide more visualizations of the learned uncertainty in Appendix E.5.

Additional analyses. We provide further analyses in the appendix. Appendix E.2 studies the effect of λ (for Eq. (8)) and (β, γ) (for Eq. (5)). Appendix E.3 reports runtime comparisons, where sampling-based baselines [10, 11] are 2.8 to 5.9 times slower than COMET in the setting. Finally, we provide an analysis of our adaptation in Appendix E.4.

6 Conclusion

We introduced COMET, a decomposition-based MLLM uncertainty estimation framework that separates context-specific ambiguity from multiplicity-specific uncertainty. By combining an MLLM-as-verifier strategy with lightweight post-hoc uncertainty heads, COMET enables efficient uncertainty estimation in open-ended multimodal settings without autoregressive answer generation or repeated sampling. Experiments across open-ended multimodal understanding, error detection, and MCQ VQA benchmarks show that this decomposition yields more reliable uncertainty estimates than existing baselines while preserving practical inference efficiency. We hope that our decomposed formulation offers a useful step toward understanding and estimating uncertainty in MLLMs.

Acknowledgements

This work is supported by the Princeton Francis Robbins Upton Fellowship to S.C. We are grateful to Allison Chen, Salma Abdel Magid, Tyler Zhu, Arnold Caleb Asimwe, and Song Park for insightful discussions and valuable feedback that helped shape this work.

References

- [1] Saurav Kadavath, Tom Conerly, Amanda Askell, Tom Henighan, Dawn Drain, Ethan Perez, Nicholas Schiefer, Zac Hatfield-Dodds, Nova DasSarma, Eli Tran-Johnson, et al. Language models (mostly) know what they know. *arXiv preprint arXiv:2207.05221*, 2022.
- [2] Stephanie Lin, Jacob Hilton, and Owain Evans. Teaching models to express their uncertainty in words. *Transactions on Machine Learning Research*, 2022. ISSN 2835-8856. URL <https://openreview.net/forum?id=8s8K2UZGTZ>.
- [3] Katherine Tian, Eric Mitchell, Allan Zhou, Archit Sharma, Rafael Rafailov, Huaxiu Yao, Chelsea Finn, and Christopher D Manning. Just ask for calibration: Strategies for eliciting calibrated confidence scores from language models fine-tuned with human feedback. In *Conference on Empirical Methods in Natural Language Processing (EMNLP)*, pages 5433–5442, 2023.
- [4] Miao Xiong, Zhiyuan Hu, Xinyang Lu, YIFEI LI, Jie Fu, Junxian He, and Bryan Hooi. Can LLMs express their uncertainty? an empirical evaluation of confidence elicitation in LLMs. In *International Conference on Learning Representations (ICLR)*, 2024. URL <https://openreview.net/forum?id=gjeQKFxFpZ>.
- [5] Wenyi Xiao, Xinchu Xu, and Leilei Gan. VL-calibration: Decoupled confidence calibration for large vision-language models reasoning. In *Association for Computational Linguistics (ACL)*, 2026.
- [6] Pranav Rajpurkar, Robin Jia, and Percy Liang. Know what you don’t know: Unanswerable questions for squad. In *Association for Computational Linguistics (ACL)*, pages 784–789, 2018.
- [7] Spencer Whitehead, Suzanne Petryk, Vedaad Shakib, Joseph Gonzalez, Trevor Darrell, Anna Rohrbach, and Marcus Rohrbach. Reliable visual question answering: Abstain rather than answer incorrectly. In *European Conference on Computer Vision (ECCV)*, pages 148–166. Springer, 2022.
- [8] Hanning Zhang, Shizhe Diao, Yong Lin, Yi Fung, Qing Lian, Xingyao Wang, Yangyi Chen, Heng Ji, and Tong Zhang. R-tuning: Instructing large language models to say ‘i don’t know’. In *Annual Conference of the North American Chapter of the Association for Computational Linguistics (NAACL)*, pages 7113–7139, 2024.
- [9] Bingbing Wen, Jihan Yao, Shangbin Feng, Chenjun Xu, Yulia Tsvetkov, Bill Howe, and Lucy Lu Wang. Know your limits: A survey of abstention in large language models. *Transactions of the Association for Computational Linguistics (TACL)*, 13:529–556, 2025.
- [10] Xuezi Wang, Jason Wei, Dale Schuurmans, Quoc Le, Ed Chi, Sharan Narang, Aakanksha Chowdhery, and Denny Zhou. Self-consistency improves chain of thought reasoning in language models. In *International Conference on Learning Representations (ICLR)*, 2023.
- [11] Ruiyang Zhang, Hu Zhang, and Zhedong Zheng. VL-Uncertainty: Detecting hallucination in large vision-language model via uncertainty estimation. *arXiv preprint arXiv:2411.11919*, 2024.
- [12] Sebastian Farquhar, Jannik Kossen, Lorenz Kuhn, and Yarin Gal. Detecting hallucinations in large language models using semantic entropy. *Nature*, 630(8017):625–630, 2024.
- [13] Joshua C Peterson, Ruairidh M Battleday, Thomas L Griffiths, and Olga Russakovsky. Human uncertainty makes classification more robust. In *International Conference on Computer Vision (ICCV)*, pages 9617–9626, 2019.
- [14] Yichun Shi and Anil K Jain. Probabilistic face embeddings. In *IEEE/CVF Conference on Computer Vision and Pattern Recognition (CVPR)*, pages 6902–6911, 2019.
- [15] Luke Vilnis and Andrew McCallum. Word representations via gaussian embedding. In *International Conference on Learning Representations (ICLR)*, 2015.
- [16] Sanghyuk Chun and Olga Russakovsky. Position: Multiplicity is an inevitable and inherent challenge in multimodal learning. In *International Conference on Machine Learning (ICML)*, 2026.

- [17] Sanghyuk Chun, Wonjae Kim, Song Park, and Sangdoon Yun. Probabilistic language-image pre-training. In *International Conference on Learning Representations (ICLR)*, 2025.
- [18] Alex Kendall and Yarin Gal. What uncertainties do we need in bayesian deep learning for computer vision? *Advances in Neural Information Processing Systems (NeurIPS)*, 30, 2017.
- [19] Dan Hendrycks and Kevin Gimpel. A baseline for detecting misclassified and out-of-distribution examples in neural networks. In *International Conference on Learning Representations (ICLR)*, 2017.
- [20] Sanyam Kapoor, Nate Gruver, Manley Roberts, Katherine Collins, Arka Pal, Umang Bhatt, Adrian Weller, Samuel Dooley, Micah Goldblum, and Andrew G Wilson. Large language models must be taught to know what they don’t know. *Advances in Neural Information Processing Systems*, 37:85932–85972, 2024.
- [21] Mehul Damani, Isha Puri, Stewart Slocum, Idan Shenfeld, Leshem Choshen, Yoon Kim, and Jacob Andreas. Beyond binary rewards: Training LMs to reason about their uncertainty. In *International Conference on Learning Representations (ICLR)*, 2026. URL <https://openreview.net/forum?id=ASQ649zdHm>.
- [22] Yash Goyal, Tejas Khot, Douglas Summers-Stay, Dhruv Batra, and Devi Parikh. Making the v in vqa matter: Elevating the role of image understanding in visual question answering. In *IEEE/CVF Conference on Computer Vision and Pattern Recognition (CVPR)*, pages 6904–6913, 2017.
- [23] Danna Gurari, Qing Li, Abigale J Stangl, Anhong Guo, Chi Lin, Kristen Grauman, Jiebo Luo, and Jeffrey P Bigham. Vizwiz grand challenge: Answering visual questions from blind people. In *IEEE/CVF Conference on Computer Vision and Pattern Recognition (CVPR)*, pages 3608–3617, 2018.
- [24] Kenneth Marino, Mohammad Rastegari, Ali Farhadi, and Roozbeh Mottaghi. Ok-vqa: A visual question answering benchmark requiring external knowledge. In *IEEE/CVF Conference on Computer Vision and Pattern Recognition (CVPR)*, pages 3195–3204, 2019.
- [25] Tianrui Guan, Fuxiao Liu, Xiyang Wu, Ruiqi Xian, Zongxia Li, Xiaoyu Liu, Xijun Wang, Lichang Chen, Furong Huang, Yaser Yacoob, et al. Hallusionbench: an advanced diagnostic suite for entangled language hallucination and visual illusion in large vision-language models. In *IEEE/CVF Conference on Computer Vision and Pattern Recognition (CVPR)*, pages 14375–14385, 2024.
- [26] Xiang Yue, Yuansheng Ni, Kai Zhang, Tianyu Zheng, Ruoqi Liu, Ge Zhang, Samuel Stevens, Dongfu Jiang, Weiming Ren, Yuxuan Sun, et al. Mmmu: A massive multi-discipline multimodal understanding and reasoning benchmark for expert agi. In *IEEE/CVF Conference on Computer Vision and Pattern Recognition (CVPR)*, pages 9556–9567, 2024.
- [27] Xiang Yue, Tianyu Zheng, Yuansheng Ni, Yubo Wang, Kai Zhang, Shengbang Tong, Yuxuan Sun, Botao Yu, Ge Zhang, Huan Sun, et al. Mmmu-pro: a more robust multi-discipline multimodal understanding benchmark (2025). In *Association for Computational Linguistics (ACL)*, 2025.
- [28] Lin Chen, Jinsong Li, Xiaoyi Dong, Pan Zhang, Yuhang Zang, Zehui Chen, Haodong Duan, Jiaqi Wang, Yu Qiao, Dahua Lin, and Feng Zhao. Are we on the right way for evaluating large vision-language models? *Advances in Neural Information Processing Systems (NeurIPS)*, 37:27056–27087, 2024.
- [29] Shuai Bai, Yuxuan Cai, Ruizhe Chen, Keqin Chen, Xionghui Chen, Zesen Cheng, Lianghao Deng, Wei Ding, Chang Gao, Chunjiang Ge, et al. Qwen3-VL technical report. *arXiv preprint arXiv:2511.21631*, 2025.
- [30] Weiyun Wang, Zhangwei Gao, Lixin Gu, Hengjun Pu, Long Cui, Xingguang Wei, Zhaoyang Liu, Linglin Jing, Shenglong Ye, Jie Shao, et al. InternVL3.5: Advancing open-source multimodal models in versatility, reasoning, and efficiency. *arXiv preprint arXiv:2508.18265*, 2025.
- [31] Lukas Aichberger, Kajetan Schweighofer, Mykyta Ielanskyi, and Sepp Hochreiter. Improving uncertainty estimation through semantically diverse language generation. In *International Conference on Learning Representations (ICLR)*, 2025.
- [32] Shengbang Tong, Ellis Brown, Penghao Wu, Sanghyun Woo, Manoj Middepogu, Sai C Akula, Jihan Yang, Shusheng Yang, Adithya Iyer, Xichen Pan, et al. Cambrian-1: A fully open, vision-centric exploration of multimodal llms. *Advances in Neural Information Processing Systems (NeurIPS)*, 37:87310–87356, 2024.
- [33] Chuan Guo, Geoff Pleiss, Yu Sun, and Kilian Q Weinberger. On calibration of modern neural networks. In *International Conference on Machine Learning (ICML)*, pages 1321–1330. PMLR, 2017.
- [34] Yarin Gal and Zoubin Ghahramani. Dropout as a bayesian approximation: Representing model uncertainty in deep learning. In *International Conference on Machine Learning (ICML)*, pages 1050–1059. PMLR, 2016.

- [35] Andrey Malinin and Mark Gales. Uncertainty estimation in autoregressive structured prediction. *arXiv preprint arXiv:2002.07650*, 2020.
- [36] Zhihong Shao, Peiyi Wang, Qihao Zhu, Runxin Xu, Junxiao Song, Xiao Bi, Haowei Zhang, Mingchuan Zhang, YK Li, Yang Wu, et al. Deepseekmath: Pushing the limits of mathematical reasoning in open language models. *arXiv preprint arXiv:2402.03300*, 2024.
- [37] Junnan Li, Ramprasaath Selvaraju, Akhilesh Gotmare, Shafiq Joty, Caiming Xiong, and Steven Chu Hong Hoi. Align before fuse: Vision and language representation learning with momentum distillation. *Advances in Neural Information Processing Systems (NeurIPS)*, 34:9694–9705, 2021.
- [38] Junnan Li, Dongxu Li, Caiming Xiong, and Steven Hoi. BLIP: Bootstrapping language-image pre-training for unified vision-language understanding and generation, 2022.
- [39] Junnan Li, Dongxu Li, Silvio Savarese, and Steven Hoi. Blip-2: Bootstrapping language-image pre-training with frozen image encoders and large language models. In *International Conference on Machine Learning (ICML)*, pages 19730–19742. PMLR, 2023.
- [40] Sanghyuk Chun, Seong Joon Oh, Rafael Sampaio De Rezende, Yannis Kalantidis, and Diane Larlus. Probabilistic embeddings for cross-modal retrieval. In *IEEE/CVF Conference on Computer Vision and Pattern Recognition (CVPR)*, 2021.
- [41] Sanghyuk Chun. Improved probabilistic image-text representations. In *International Conference on Learning Representations (ICLR)*, 2024.
- [42] Aishwarya Agrawal, Dhruv Batra, Devi Parikh, and Aniruddha Kembhavi. Don’t just assume; look and answer: Overcoming priors for visual question answering. In *IEEE/CVF Conference on Computer Vision and Pattern Recognition (CVPR)*, pages 4971–4980, 2018.
- [43] Remi Cadene, Corentin Dancette, Matthieu Cord, and Devi Parikh. Rubi: Reducing unimodal biases for visual question answering. In *Advances in Neural Information Processing Systems (NeurIPS)*, volume 32, 2019.
- [44] Christopher Clark, Mark Yatskar, and Luke Zettlemoyer. Don’t take the easy way out: Ensemble based methods for avoiding known dataset biases. In *Proceedings of the 2019 conference on empirical methods in natural language processing and the 9th international joint conference on natural language Processing (EMNLP-IJCNLP)*, pages 4069–4082, 2019.
- [45] Hyojin Bahng, Sanghyuk Chun, Sangdoon Yun, Jaegul Choo, and Seong Joon Oh. Learning de-biased representations with biased representations. In *International Conference on Machine Learning (ICML)*, 2020.
- [46] Haotian Liu, Chunyuan Li, Qingyang Wu, and Yong Jae Lee. Visual instruction tuning. *Advances in Neural Information Processing Systems (NeurIPS)*, 36:34892–34916, 2023.
- [47] Alec Radford, Jong Wook Kim, Chris Hallacy, Aditya Ramesh, Gabriel Goh, Sandhini Agarwal, Girish Sastry, Amanda Askell, Pamela Mishkin, Jack Clark, Gretchen Krueger, and Ilya Sutskever. Learning transferable visual models from natural language supervision. In *International Conference on Machine Learning (ICML)*, pages 8748–8763. PMLR, 2021.
- [48] Ashish Vaswani, Noam Shazeer, Niki Parmar, Jakob Uszkoreit, Llion Jones, Aidan N Gomez, Łukasz Kaiser, and Illia Polosukhin. Attention is all you need. In *Advances in Neural Information Processing Systems (NeurIPS)*, pages 5998–6008, 2017.
- [49] Byeongho Heo, Sanghyuk Chun, Seong Joon Oh, Dongyoon Han, Sangdoon Yun, Gyuwan Kim, Youngjung Uh, and Jung-Woo Ha. AdamP: Slowing down the slowdown for momentum optimizers on scale-invariant weights. In *International Conference on Learning Representations (ICLR)*, 2021.
- [50] Nitish Srivastava, Geoffrey Hinton, Alex Krizhevsky, Ilya Sutskever, and Ruslan Salakhutdinov. Dropout: a simple way to prevent neural networks from overfitting. *Journal of machine learning research (JMLR)*, 15(1):1929–1958, 2014.
- [51] Ziang Zhou, Tianyuan Jin, Jieming Shi, and Qing Li. Steerconf: Steering llms for confidence elicitation. *arXiv preprint arXiv:2503.02863*, 2025.
- [52] Edward J Hu, yelong shen, Phillip Wallis, Zeyuan Allen-Zhu, Yuanzhi Li, Shean Wang, Lu Wang, and Weizhu Chen. LoRA: Low-rank adaptation of large language models. In *International Conference on Learning Representations (ICLR)*, 2022. URL <https://openreview.net/forum?id=nZeVKeeFYf9>.

- [53] Yibo Li, Miao Xiong, Jiaying Wu, and Bryan Hooi. Conftuner: Training large language models to express their confidence verbally. *arXiv preprint arXiv:2508.18847*, 2025.
- [54] Anita Kriz, Elizabeth Laura Janes, Xing Shen, and Tal Arbel. Prompt4trust: A reinforcement learning prompt augmentation framework for clinically-aligned confidence calibration in multimodal large language models. In *International Conference on Computer Vision Workshop (ICCVW)*, pages 1320–1329, 2025.
- [55] Jason Wei, Xuezhi Wang, Dale Schuurmans, Maarten Bosma, Fei Xia, Ed Chi, Quoc V Le, Denny Zhou, et al. Chain-of-thought prompting elicits reasoning in large language models. *Advances in Neural Information Processing Systems (NeurIPS)*, 35:24824–24837, 2022.
- [56] Changdae Oh, Seongheon Park, To Eun Kim, Jiatong Li, Wendi Li, Samuel Yeh, Xuefeng Du, Hamed Hassani, Paul Bogdan, Dawn Song, and Sharon Li. Uncertainty quantification in llm agents: Foundations, emerging challenges, and opportunities. In *Association for Computational Linguistics (ACL)*, 2026.

Appendix

A More Related Work

Uncertainty estimation. Uncertainty estimation has been studied in deep neural networks. Early works in closed-set tasks (*e.g.*, classification) focused on predicting uncertainty scores based on their prediction probability, *e.g.*, entropy [18] or softmax confidence score [19]. These methods have demonstrated effectiveness on calibration [33] or out-of-distributed data detection [19]. However, if the answer space is not explicitly given, these methods are no longer applicable.

Improving uncertainty estimation via fine-tuning. Although using M/LLM as uncertainty estimator empirically shows meaningful uncertainty estimation, these methods need additional fine-tuning of the backbone LM [20, 5] to achieve a proper uncertainty estimate in practice. This introduces additional training cost and may degrade the generalizability of the original M/LLMs. COMET aims to estimate uncertainty of a frozen MLLM by employing lightweight post-hoc uncertainty heads, resulting in efficient uncertainty estimation.

Uncertainty decomposition. A classical line of work decomposes predictive uncertainty into aleatoric uncertainty, which captures data uncertainty (how data itself is uncertain), and epistemic uncertainty (how the trained model is uncertain) [18, 34, 35]. Our decomposition is fundamentally different in its target and motivation. Rather than separating data noise from model uncertainty, we study semantic predictive uncertainty in open-ended multimodal settings, where the answer space is not explicitly enumerable and multiple semantically valid answers may exist for the same input and context. In our formulation, the context-specific term measures how broadly the context t defines the plausible answer space, while the multiplicity-specific term measures how many of those context-plausible answers remain compatible with the observed input x . Thus, our decomposition is not an aleatoric-epistemic decomposition of model uncertainty, but a semantic decomposition of answer-space uncertainty induced by context and input-answer compatibility. We argue that this distinction is important for MLLMs, because uncertainty can remain high even with a fixed frozen model, not because the model parameters are uncertain, but because the context induces many valid answers or the input supports multiple compatible answers under the context.

Concurrent with our work, Xiao et al. [5] proposed a decoupled multimodal uncertainty estimation framework that combines perturbation-based visual grounding confidence [11] with reasoning-side internal confidence based on token entropy. Unlike our method, their formulation is built on heuristic confidence proxies rather than theoretically motivated quantity. For example, there is no specific reason of why the uncertainty should be decomposed into those two quantities, and why each quantity can be measured by the proposed quantities. Furthermore, their approach focuses on reasoning-oriented MLLMs and requires backbone fine-tuning based on GRPO [36], whereas our method estimates uncertainty for general-purpose MLLMs using lightweight post-hoc modules on top of a frozen backbone.

B More discussions on uncertainty decomposition

B.1 Why Rényi entropy?

As we discussed in the main paper, when the output space is unknown or continuous, the standard discrete Shannon entropy is not directly applicable. One may consider the differential entropy ($H_d := \mathbb{E}_{Y \sim \pi_Y}[-\log \pi_Y]$) as an alternative, but it is not aligned with our desired property. More specifically, differential entropy measures the spread of a continuous density with respect to a chosen reference measure. In open-ended answer spaces, any continuous representation of answers is largely arbitrary, so differential entropy would depend on representational choices rather than directly reflecting the multiplicity of semantic answers.

Assume an open-ended answer distribution has one dominant region of plausible answers with a tail of low-probability variants (illustrated in Fig. B.1). In this case, even though we fix the total probability mass assigned to the tail, by enlarging the tail support, the differential entropy is increased without bound (See Eq. (B.1)). Instead, a proper uncertainty estimate should more directly reflect the

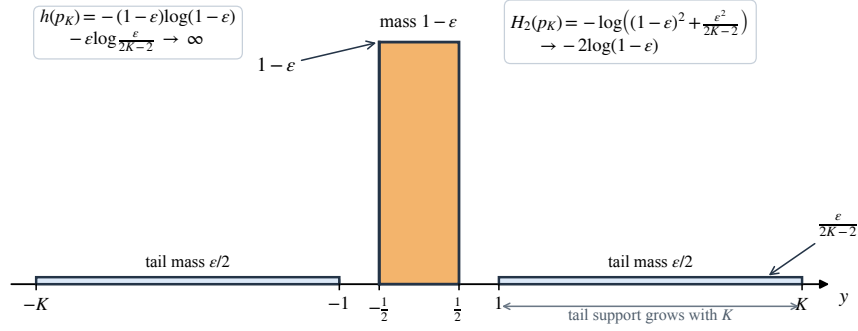


Figure B.1: **A counterexample for differential entropy.** The distribution p_K has one dominant region of mass $1 - \epsilon$ and diffuse tails with total mass ϵ spread over growing support. Differential entropy diverges as $K \rightarrow \infty$, even though the high-probability semantic region remains unchanged, whereas Rényi-2 remains bounded and converges to $-2 \log(1 - \epsilon)$.

concentration of probability mass on the core plausible answers.

$$H(p(x)) = - \int p(x) \log p(x) dx = -(1-\epsilon) \log(1-\epsilon) - \epsilon \log \frac{\epsilon}{2k-2} \quad \text{if } k \rightarrow \infty, H \rightarrow \infty \quad (\text{B.1})$$

On the other hand, Rényi-2 entropy remains bounded even when its tail spreads over an increasingly wide support (See Eq. (B.2)); whereas differential entropy diverges in the same setting. Therefore, it better reflects the concentration of probability mass on the core plausible answers.

$$H_2(p(x)) = - \log \int p(x)^2 dx = - \log\left((1-\epsilon)^2 - \frac{\epsilon^2}{2k-2}\right) \quad \text{if } k \rightarrow \infty, H_2 \rightarrow -2 \log(1-\epsilon) \quad (\text{B.2})$$

B.2 The full derivation of uncertainty decomposition with Rényi-2 entropy

We denote $s(x, t, y) := p(m = 1 | x, t, y)$ for simplicity. We also assume that $p(y | t)$ is a uniform distribution over a restricted region Ω , namely $p(y | t) = \frac{1}{\int_{\Omega} dy} = \frac{1}{K_t}$. Now, we define the first and the second moments of the matching probability over $p(y | t)$ as follows:

$$\begin{aligned}
 Z_1(x, t) &:= \mathbb{E}_{Y \sim p(\cdot | t)} [s(x, t, Y)] = \int s(x, t, y) p(y | t) dy \\
 Z_2(x, t) &:= \mathbb{E}_{Y \sim p(\cdot | t)} [s(x, t, Y)^2] = \int s(x, t, y)^2 p(y | t) dy = \frac{1}{K_t} \int s(x, t, y)^2 dy
 \end{aligned} \quad (\text{B.3})$$

From the definition of Rényi-2 entropy, we can derive the following decomposition:

$$\begin{aligned}
 u(x, t) &:= H_2(\pi_y) = - \log \int \pi_y^2 dy = - \log \int \frac{s(x, t, y)^2 p(y | t)^2}{Z_1(x, t)^2} dy \\
 &= - \log \left[\frac{1}{K_t^2} \frac{1}{Z_1(x, t)^2} \int s(x, t, y)^2 dy \right] = - \log \left[\frac{1}{K_t} \frac{Z_2(x, t)}{Z_1(x, t)^2} \right] \\
 &= \underbrace{\log K_t}_{:=u_t(t)} + \underbrace{2 \log Z_1(x, t) - \log Z_2(x, t)}_{:=u_{x|t}(x|t)} \\
 &= \underbrace{\log K_t}_{:=u_t(t)} + \underbrace{\left(- \log \left[\frac{\text{Var}(s)}{(\mathbb{E}(s))^2} + 1 \right] \right)}_{:=u_{x|t}(x|t)} = \underbrace{\log K_t}_{:=u_t(t)} + \underbrace{\left(- \log [\text{CV}(s)^2 + 1] \right)}_{:=u_{x|t}(x|t)},
 \end{aligned} \quad (\text{B.4})$$

where $\text{CV}(\cdot)$ denotes the coefficient of variance (also known as normalized root-mean-square deviation), which is defined as follows:

$$\text{CV}(s) = \frac{\sqrt{\text{Var}(s)}}{\mathbb{E}(s)} = \sqrt{\frac{\mathbb{E}[s^2]}{\mathbb{E}[s]^2} - 1} = \sqrt{\frac{Z_2}{Z_1^2} - 1}. \quad (\text{B.5})$$

Eq. (B.4) implies that the uncertainty of an input x with a given task t is given by the summation of (1) how the output space is complex ($\log K_t$), and (2) the negative coefficient of variance (also known as normalized root-mean-square deviation) of the matching probability $s(x, t, y)$. Namely, it measure how the matching probability between the input x and the answer set \mathcal{Y} under the context t is distributed. Therefore, $u_{x|t}$ measures the degree of many-to-many relationships or multiplicity [16] of the matching between x and y . For example, if we have more plausible answers compatible to the given x under t , the uncertainty will be higher.

B.3 Derivation of Shannon's entropy in a discrete case

Now, we assume that the answer space y is discrete and explicitly enumerable. In this case, we can derive the following equation from the definition of discrete entropy:

$$\begin{aligned} H(\pi_y) &= -\sum_y \pi_y \log \pi_y = -\sum_y \pi_y (\log s + \underbrace{\log p(y|t)}_{\text{constant}} - \log Z_1(x, t)) \\ &= \log K_t - \sum_y \pi_y \log s + \sum_y \pi_y \log \underbrace{Z_1(x, t)}_{=\mathbb{E}[s]} = \log K_t - \sum_y \pi_y \log s + \log(\mathbb{E}_{Y \sim p(\cdot|t)}[s]) \end{aligned} \quad (\text{B.6})$$

Note that $\sum_y \pi_y \log \mathbb{E}[s] = \log \mathbb{E}[s] \sum_y \pi_y = \log \mathbb{E}[s]$, because $\mathbb{E}[s]$ is no longer a function of y . Here, we rewrite $-\sum_y \pi_y \log s$ as follows:

$$-\sum_y \pi_y \log s = -\frac{1}{Z_1} \sum_y s \log s \cdot p(y|t) = -\frac{1}{Z_1} \mathbb{E}_{Y \sim p(\cdot|t)}[s \log s]. \quad (\text{B.7})$$

Therefore, we have $H(\pi_y) = \log K_t + \log Z_1 - \frac{1}{Z_1} \mathbb{E}_{Y \sim p(\cdot|t)}[s \log s]$. We approximate this value using a second-order Taylor expansion. Let $\mu = \mathbb{E}[s]$ and $s = \mu + \delta$, where $\mathbb{E}[\delta] = 0$, $\mathbb{E}[\delta^2] = \sigma^2$. Now, apply the Taylor expansion to $f(s) = s \log s$ and take the expectation as follows:

$$\begin{aligned} \mathbb{E}_{Y \sim p(\cdot|t)}[s \log s] &= \mathbb{E}[f(\mu + \delta)] \approx \mathbb{E}\left[\mu \log \mu + (1 + \log \mu)\delta + \frac{\delta^2}{2\mu}\right] \\ &= \mu \log \mu + \mathbb{E}[\delta](1 + \log \mu) + \frac{\mathbb{E}[\delta^2]}{2\mu} = \mu \log \mu + \frac{\sigma^2}{2\mu} = Z_1 \log Z_1 + \frac{Z_2 - Z_1^2}{2Z_1}. \end{aligned} \quad (\text{B.8})$$

Substituting this into Eq. (B.6), we have:

$$\begin{aligned} H(\pi_y) &= \log K_t + \log Z_1 - \frac{1}{Z_1} \mathbb{E}_{Y \sim p(\cdot|t)}[s \log s] \\ &= \log K_t + \log Z_1 - \log Z_1 - \frac{1}{2} \frac{Z_2}{Z_1^2} = \log K_t - \frac{1}{2} \left(\frac{Z_2}{Z_1^2} - 1 \right) \end{aligned} \quad (\text{B.9})$$

Interestingly, Eq. (B.9) is very similar to the formulation derived from Rényi-2 entropy in Appendix B.2 (the constant term is omitted):

$$H(\pi_y) \approx \log K_t - \frac{1}{2} \frac{Z_2}{Z_1^2} = \underbrace{\log K_t}_{:=u'_t(t)} + \underbrace{\left(-\frac{1}{2} \frac{\text{Var}(s)}{(\mathbb{E}[s])^2}\right)}_{:=u'_{x|t}(x|t)} \quad (\text{B.10})$$

$$H_2(\pi_y) = \log K_t - \log \frac{Z_2}{Z_1^2} = \underbrace{\log K_t}_{:=u_t(t)} + \underbrace{\left(-\log \left[\frac{\text{Var}(s)}{(\mathbb{E}(s))^2} + 1 \right]\right)}_{:=u_{x|t}(x|t)} \quad (\text{B.11})$$

Both imply the same intuition: the uncertainty of the posterior π_y is decomposed by (1) the task-dependent uncertainty value $\log K_t$, *i.e.*, how the possible outcome space is large and complex, and (2) the uncertainty value by input and task, related to the normalized standard deviation of the matching probability $p(m = 1 | x, t, y)$ over all the possible outcome y for a given task t , $\text{CV}_{Y \sim p(\cdot|t)}[s(x, t, y)]$. The Shannon information entropy is directly related to the normalized standard deviation, while Rényi entropy is related to the log of the value.

C Method details

C.1 Details of MLLM-as-verifier

Our decomposition requires a matching probability function $p(m = 1 | x, t, y)$. We can employ a parameterized matching probability module, which is a binary classifier that takes a (x, t, y) triplet as input. This strategy is popular in vision-language models (VLMs) training, *e.g.*, image-text matching (ITM) loss [37–39] or directly optimizing the loglikelihood of the matching probability between vision-language embeddings [40, 41, 17]. However, we found that training a reliable matching probability module is difficult for two reasons. First, it easily suffers from the context shortcut similar to the text-shortcut problem in early visual-question answering (VQA) tasks [42–45]. Also, we need a large-scale (x, t, y) triplet dataset to train a matching probability module; however, we empirically found that a matching probability module trained on a triplet dataset, such as visual instruction tuning dataset [46, 32] does not generalize to arbitrary open-ended settings.

For example, we can achieve this by using a contrastive loss [47], *i.e.*, treating the answers corresponding to the original x, t as positives and all the other answers from the other x, t in the mini-batch as negatives. However, we found that 84% the questions in the Cambrian dataset are unique, *i.e.*, if we apply contrastive learning to this dataset, the learned module is highly motivated to simply determine the matching based on t , while ignoring x .

Table C.1: Unique answers per question in Cambrian dataset [32].

# Unique answers	1	2	3–5	6–10	11–20	21–50	>50
# samples	811,806	120,364	22,470	7,038	2,615	945	250

As a probing example, we train a simple MLP that estimates whether the given x, t and y are matched upon CLIP-L/14 features [47]. When we test the module on the separated validation split with the same distribution with the training dataset, it shows 0.97 AUROC; however, when we mix the questions across the validation dataset, so each test question now can appear with random answers, the AUROC drops significantly to 0.51, which is almost random. In other words, it is very difficult to train matching probability module because the text short between t and y could happen.

C.2 Prompt for verification-based matching probability

Fig. C.1 shows the prompt template for our MLLM-as-verifier matching probability.

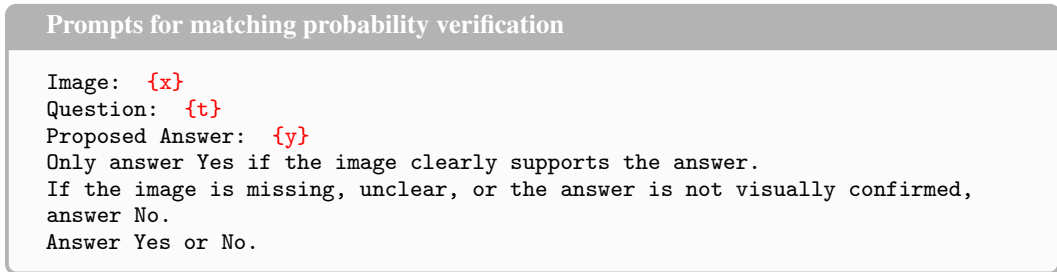


Figure C.1: Prompt for MLLM-based matching probability.

Using this template, we measure the $p(y = \text{“Yes”} | x, t)$ and $p(y = \text{“No”} | x, t)$ to compute the matching probability using Eq. (5).

C.3 Matching probability calibration

Recall that Eq. (5) needs affine transform variables, β and γ . This affine transform does not change the order of matching probabilities (because this is a monotonic increasing function), but it calibrates the degree of matching probability; smaller β makes the distribution of matching probability smoother, and γ controls a “reference point” for matching probability (*i.e.*, it shifts the distribution).

We apply a simple optimization to get a calibrated affine transform. We first binarize the distribution using a threshold, *i.e.*, $m = 1$ if $p(m) > 0.5$, otherwise 0, and search for β, γ that achieves the best matching accuracy in the validation dataset. We use the MMMU validation split for the calibration; because MMMU is a MCQ dataset, there exist positive samples (where $m = 1$) and negative samples (where $m = 0$) for each x and t . We achieve the best matching accuracy with $\beta = 0.2$ and $\gamma = -0.1$ for Qwen3VL-2B-Instruct. We use the same value for all the other backbones, such as Qwen3VL-4B and 8B models, and the InternVL model.

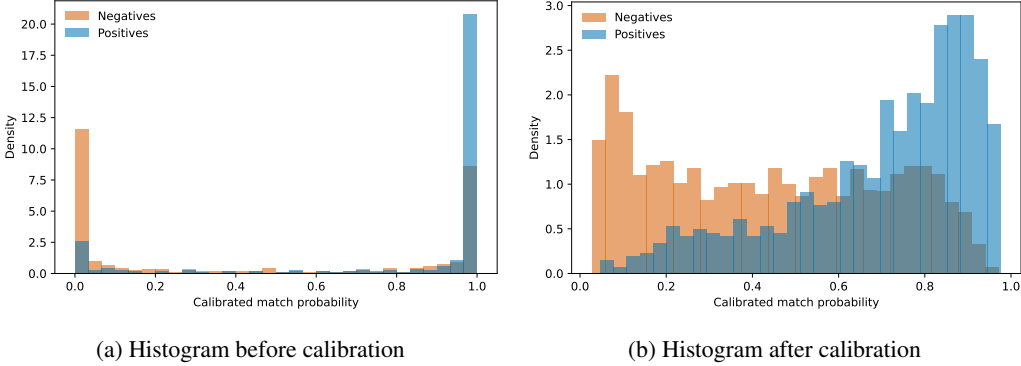


Figure C.2: **Matching probability histogram before and after calibration.** We visualize the matching probability distributions in the MMMU [26] validation split. The blue bars denote the matching probability distribution for the triplet (x, t, y_+) where y_+ is the corresponding answer among the given multiple-choice questions. The orange bars denote the matching probability when a negative answer is given.

Fig. C.2 shows the distribution of matching probabilities on the MMMU validation split before and after calibration, *i.e.*, before calibration means $\beta = 1, \gamma = 0$ and after calibration means $\beta = 0.2$ and $\gamma = -0.1$. As we discussed previously, the calibration makes the overall matching probability distribution smoother.

In a later section, we will show that this calibration strategy achieves a better uncertainty estimation in the MMMU validation split (where we optimize the hyperparameter) as well as the target benchmark – See Tab. E.5 for more details.

C.4 Dataset collection details

For dataset collection, we first perform the text clustering described in Fig. C.3 to get plausible answers for each question. We compute the similarity between texts using the CLIP-L/14 text encoder [47]. After that, we randomly select 200,000 rows from the Cambrian dataset. For each example (x_i, t_i, y_i^+) assigned to the prototype p_i , we construct a candidate set \mathcal{Y}_i containing the original answer and prototype positives (*i.e.*, answers corresponding to the other questions in the same cluster). Due to the computation complexity, we restrict the size of \mathcal{Y}_i to 32 in our experiments.

Then, we extract the following features for our training: (1) $f_\theta(x_i, t_i)$: the MLLM feature of the input pair x_i and t_i , (2) $f_\theta(t_i)$: the MLLM feature of the input t_i , (3) $\log p(\text{“Yes”} \mid x_i, t_i, y_i^+)$ for Eq. (5) – this value is computed for all candidates $y_i \in \mathcal{Y}_i$; we also extract the log probability of “No”, and (4) $\log p(y_i \mid t_i)$ for all candidates $y_i \in \mathcal{Y}_i$. These values are used to estimate the targets $\hat{Z}_1(x, t)$, $\hat{Z}_2(x, t)$ and $\hat{u}(x, t)$, and for input features of the uncertainty estimation modules F_{Z_1}, F_{Z_2} and F_{u_t} . In practice, we pre-extracted features and re-use the pre-computed values for training to reduce the computation cost due to the MLLM inference.

C.5 Training and architecture details

We employ three neural uncertainty estimation modules $F_{Z_1}(x, t)$, $F_\Delta(x, t)$ and $F_{u_t}(t)$ that estimate $\log \hat{Z}_1(x, t)$, $\Delta = \log \hat{Z}_1(x, t) - \log \hat{Z}_2(x, t)$ and $\hat{u}_t(t)$, respectively. Here, Δ is always nonnegative because $0 \leq p(m = 1 \mid x, t, y) \leq 1$. We use a lightweight Transformer architecture for the uncertainty modules. We use a Transformer for estimating $F_{Z_1}(x, t)$ and $F_\Delta(x, t)$ by taking the MLLM features of (x, t) and t ($f_\theta(x, t)$ and $f_\theta(t)$, respectively) for their input. $F_{u_t}(t)$ is also a

```

1 def greedy_clustering(dataset, sim_fn, thres):
2     """dataset: (x, t, y) triplets
3         sim_fn: text similarity function (higher is more similar) """
4     # Collect answers by question/context.
5     candidates = {}
6     for x, t, y in dataset:
7         candidates[t].append(y)
8
9     # Process frequent questions first.
10    candidates = sorted(
11        candidates.items(),
12        key=lambda item: len(item[1]),
13        reverse=True,
14    )
15
16    clusters = []
17    cluster_assignments = {}
18    for t, answers in candidates:
19        # Greedy cluster assignment to the first similar cluster.
20        assigned = False
21        for cluster in clusters:
22            if sim_fn() > thres:
23                cluster_assignments[cluster].extend(answers)
24                assigned = True
25                break
26
27        if not assigned:
28            # Ensure that the order of clusters is sorted by the frequency.
29            clusters.append(t)
30            cluster_assignments[t] = answers
31    return cluster_assignments

```

Figure C.3: Greedy clustering Python pseudo-code.

Transformer, which takes $f_\theta(t)$ as its input. These modules are all 3-layer multi-head Transformers [48] with a hidden dimension of 768 and 8 attention heads. The outputs are pooled by an attention pooling, and then fed into a linear head to estimate the target value; $F_{Z_1}(x, t)$ and $F_\Delta(x, t)$ share the Transformer backbone, but use different attention pooling modules and the linear projection. Since Z_1 and Z_2 are the first and second momentum of probability $\in [0, 1]$, the output of F_{Z_1} and F_Δ should be in $(-\infty, 0]$; we use a softplus operation to ensure their value range. This is a similar technique to enforce positive variance values in probabilistic embeddings [40, 41, 17].

As we briefly described in Appendix C.4, we use the mixture of the pooled features for the input of our module. More specifically, F_{Z_1} takes $f(x, t)$, the MLLM feature of multimodal input (x, t) , and $f(t)$, the MLLM feature of text-only input (t) . We use four pooled feature types for these features: (1) the last output token – which is also known as “end of sentence (EOS)” token [47], (2) the mean of the last eight output tokens, (3) the mean of the last 32 output tokens, and (4) the mean of the entire output tokens. We pre-extract these values from the dataset and cache them to avoid expensive MLLM forward operations. These four features are fed into the Transformer; F_{Z_1} and F_Δ take 16 token features as their input (four features from each $f(x, t)$, $f(t)$, $f(x, t) - f(t)$, and $f(x, t) \times f(t)$), while F_{u_t} takes four tokens as input.

During training, we optimize the following objective function using a regression loss ℓ (e.g., ℓ_1 loss) on collected data samples described in Sec. 4.2:

$$\ell(F_{Z_1}(x, t), \log \hat{Z}_1(x, t)) + \ell(F_\Delta(x, t), \Delta) + \ell(\lambda F_{u_t}(t) + F_{Z_1}(x, t) + F_\Delta(x, t), \hat{u}(x, t)). \quad (\text{C.1})$$

Since our training dataset has a different distribution from the actual target benchmarks, we found that the modules trained on our collected training dataset using Eq. (C.1) often suffer from the generalizability problem. To mitigate this issue, we additionally employ a lightweight adaptation to a small number of data samples related to the target benchmark. Let \mathcal{I}^+ denote the set of samples (x_i, t_i, y_i) that are correctly predicted by an MLLM and \mathcal{I}^- denote the set of incorrectly predicted samples. The adaptation loss is defined as follows:

$$\mathbb{E}_{i \in \mathcal{I}^+, j \in \mathcal{I}^-} [-\text{softplus}(u'_j - u'_i)], \quad \text{where } u'_i := \lambda F_{u_t}(t_i) + \log F_{Z_1}(x_i, t_i) + F_\Delta(x_i, t_i). \quad (\text{C.2})$$

Table D.1: **Overview of evaluation benchmarks.** The detailed statics of the datasets are shown. We report the number of samples for each dataset and its answer type. We also report the performance of Qwen3VL-2B, -4B, -8B-Instruct models and InternVL3.5-1B model on each dataset. For open-ended VQAs, we report the original VQA score and separately report the threshold-based accuracy used in our experiments in the brackets. †: The original VQA v2 has 214,354 images, but we randomly select 10k samples for our evaluation. ‡: These samples are used for the adaptation. *: These samples are used for model selection and hyperparameter tuning.

	Dataset stats		Performance			
	# Samples	Answer type	Qwen 2B	Qwen 4B	Qwen 8B	Intern 1B
VQA v2 (Validation) [22]	10,000 [†]	Open-ended	62.2 (61.6)	82.8 (82.5)	71.6 (71.3)	76.5 (76.0)
VQA v2 (Adaptation)	10,000 [‡]	Open-ended	-	-	-	-
Vizwiz (Validation) [23]	4319	Open-ended	38.9 (37.2)	46.4 (45.0)	40.8 (39.3)	41.2 (39.0)
OK-VQA (Validation) [24]	5046	Open-ended	46.1 (49.3)	61.2 (64.8)	55.4 (58.5)	54.9 (59.0)
HallusionBench [25]	1129	Yes / No	40.4	61.2	61.5	45.6
MMMU (Test) [26]	10500	MCQ	26	43.4	47.5	37.4
MMMU (Validation)	900 ^{‡*}	MCQ	-	-	-	-
MMMU (Dev)	150*	MCQ	-	-	-	-
MMMU Pro [27]	1730	MCQ	20.6	32.2	35.9	28
MMStar [28]	1500	MCQ	41.5	48.3	49.3	39.1

Eq. (C.2) calibrates the predicted uncertainty value using the actual prediction of an MLLM by enlarging the gap between the uncertainty of correctly predicted samples and that of incorrect samples. For our experiments, we use 1k multiple choice question VQA samples from the MMMU dataset [26] and 10k open-ended VQA samples for the adaptation from the VQA v2 dataset [22].

D More Experimental Setup

D.1 Evaluation dataset details

We report the details of each dataset in Tab. D.1. Note that the uncertainty estimation methods compared in this paper keep the backbone MLLM weight frozen; therefore, their performance on each dataset are identical each other. In the main paper, we use 10,000 randomly sampled VQA v2 samples for reporting the VQA v2 results to reduce the expensive inference cost by generation-based methods ([†] in the table). We also use randomly selected (but mutually exclusive) 10k samples from VQA v2 and 900 MMMU validation samples for our lightweight adaptation ([‡] in the table). Finally, 150 MMMU dev samples and 900 MMMU validation samples are used for model selection and hyperparameter tuning along with the 1k validation split from our collected samples (Sec. 4.2).

In the table, the performances are measured by (1) a soft VQA score [22] for open-ended VQAs and (2) accuracy for the other tasks. Here, we additionally report the threshold-based accuracy for open-ended VQA tasks, which will be described in the following subsection.

D.2 Evaluation metric details

We use the following three metrics as our main metrics: AUROC, AUPRC and FPR95 (False Positive Rate when the True Positive Rate is 95%), which are standard metrics to measure the performance of uncertainty estimates [19].

These metrics are defined based on a binary classifier where the input is uncertainty score and the output is whether prediction is correct or incorrect. However, for open-ended VQA tasks, we use a soft score, named VQA score [22] as $\min\left(\frac{m(y)}{3}, 1\right)$, where $m(y)$ is the number of human reference answers that match the model prediction y after normalization. The main numbers in Tab. D.1 are the average VQA score over the samples.

To measure the uncertainty estimation performance of each method, we make the soft VQA score to a binary 0, 1 value using a threshold, *i.e.*, if the score is larger than threshold τ , the score becomes 1, otherwise 0. We report the accuracy measured by this in Tab. D.1 (numbers in brackets).

```

Prompts for comparison methods

[Loglikelihood]
Image: {x}
Question: {t}
Proposed Answer: {y}

[Verbalized Confidence]
Image: {x}
Question: {t}
Proposed Answer: {y}
How likely is the possible answer to be correct? Briefly explain, then write
only one score from 0 to {confidence_scale} inside <confidence></confidence>
tags.
Answer Yes or No.

[P(Correct)]
Image: {x}
Question: {t}
Proposed Answer: {y}
Is the proposed answer correct?
(A) True
(B) False
The proposed answer is:

```

Figure D.1: Prompts for comparison methods.

D.3 Implementation details

We optimize the uncertainty modules using AdamP [49] with a learning rate of 10^{-5} , a batch size of 64, weight decay of 0, and a dropout ratio [50] of 0.1. We optimize the module for 50 epochs and choose the best model based on the validation AUROC using the 1k held-out split. For hyperparameters, we search over λ in $\{0.25, 0.5, 1.0\}$ based on the MMMU validation split (MMMU val AUROC – MMMU val FPR95). Based on this, $\lambda = 0.25$ was selected as the best hyperparameter except for Qwen3VL-4B, where its best λ is 1.0.

During training, for each iteration, we randomly sample 16 samples from 32 samples of plausible answers. (described in Sec. 4.2).

For the lightweight adaptation stage, we search over batch size in $\{128, 256, 512\}$ and learning rate in $\{10^{-3}, 5 \times 10^{-4}, 10^{-4}, 5 \times 10^{-5}\}$ for each trained uncertainty module. Adaptation is also run for up to 50 epochs, and the best checkpoint is selected based on development-set AUROC.

D.4 Comparison methods details

Negative log-likelihood (NLL). NLL uses the likelihood of the generated answer under the backbone model as a confidence proxy. Lower likelihood corresponds to higher uncertainty. This is a natural decoder-based baseline but is often sensitive to output length and tokenization.

$$\ell(x, t, y) := - \sum_{i=1}^{|y|} \log p_{\theta}(y_i | x, t, y_{<i}). \tag{D.1}$$

In our experiments, however, we found that NLL actually does not serve as a proper uncertainty estimate; it usually shows a very low AUROC score, which means that higher likelihood corresponds to higher uncertainty. This is contradictory to our intuition, and it supports that naively using MLLM output as uncertainty estimate may not work very well in practice.

P(Correct). Following Kadavath et al. [1], we ask the model a follow-up verification question about its own answer and use the probability of the affirmative response as a confidence score (See Fig. D.1 for the prompt). This baseline is closely related to our verifier, but it is applied to the model’s final generated answer rather than to a candidate-answer bank used to construct uncertainty moments.

Verbalized confidence. We also compare against verbalized confidence [3], where the model is prompted to explicitly state a confidence value in natural language. This baseline tests whether self-reported confidence alone is sufficient for reliable uncertainty estimation.

VL-Uncertainty. VL-Uncertainty [11] measures uncertainty from the stability of model outputs under multimodal perturbations. It is a strong multimodal baseline, but it is substantially more expensive than our single-pass estimator because it requires multiple perturbed forward passes and repeated generation. In our implementation, we use five perturbation rounds, pairing image blur radius $\{0.6, 0.8, 1.0, 1.2, 1.4\}$ with question-rephrasing temperatures $\{0.1, 0.2, 0.3, 0.4, 0.5\}$. For each perturbed input, we sample an answer with temperature 1.0, $\text{top-}p = 0.9$, and at most 32 new tokens, cluster the sampled answers into semantic groups, and use the entropy of the cluster-count distribution as the uncertainty score.

Consistency-based baselines. Following Wang et al. [10], we sample multiple answers for the same input and build an empirical answer distribution from the normalized outputs. We then compute either the entropy of this distribution or its maximum probability. These baselines are effective when short answers repeat reliably, but they become less stable when valid answers can be paraphrased in many ways. In our experiments, we sample five answers with temperature 1.0, $\text{top-}p = 0.9$, and at most 32 new tokens. Then we count the normalized output to make a multinomial distribution; entropy and maximum probability are used for uncertainty score.

Candidate-based baselines. For MCQ benchmarks, we additionally report candidate-based baselines computed over the explicit answer options. More specifically, we compute the log probability of each candidate (Eq. (D.1)) and use the value as the logit of the candidate; then we get a softmax probability using the logit values. These baselines are not candidate-free, but they provide a useful reference point in settings where the answer set is fully specified at test time.

We consider SteerConf [51] as well, which is a prompt-based baseline that queries the model multiple times under different confidence styles (*e.g.*, from very cautious to very confident). SteerConf extracts an answer-confidence pair from each response, and then aggregates these responses into a calibrated uncertainty estimate. When we applied SteerConf in our settings, it only produces a valid score when the model follows the required output format reliably enough across several steering levels. Concretely, many responses do not contain a parsable answer-confidence pair, therefore, it often fails to predict uncertainty score; we therefore did not compare SteerConf with COMET.

We also did not compare COMET with methods that require additional fine-tuning (or LoRA adaptation [52]) on the model, *e.g.*, Kapoor et al. [20], ConfTuner [53], Prompt4Trust [54], RLCR [21], or VL-Calibration [5]. We aim to keep the original weight of MLLM fixed and measure the uncertainty of the given MLLM without any model steering. These methods may improve calibration by changing the model itself, often with extra supervision, optimization, and hyperparameter tuning, and are therefore not directly comparable to a frozen-weight post-hoc uncertainty estimator.

Finally, it is worth noting that COMET does not need to generate y , but only takes x and t as its input for uncertainty estimation (Appendix C.5) during inference time, resulting in more efficient uncertainty estimation than the comparison methods.

E More Experiment Results

E.1 Full results

We show the full results of open-ended multimodal understanding benchmarks (Tab. E.1), unanswerability/hallucination detection benchmarks (Tab. E.2), and multiple choice question (MCQ) visual question answering (VQA) benchmarks (Tab. E.3).

E.2 Parameter study

Tab. E.4 and Tab. E.5 show the parameter study results on λ and (β, γ) using the Qwen3VL-8B-Instruct model. We select the best hyperparameter based on the MMMU validation split. In the tables, we observe that our hyperparameter choice performs the best on the MMMU validation split as well as the average score.

Table E.1: **Open-ended VQA results.** We report AUROC (AUC), AUPRC (AP), and FPR@95 of uncertainty estimation methods on open-ended VQA benchmarks. “GF” denotes generation-free.

Method	Qwen3VL-2B-Instruct			Qwen3VL-4B-Instruct			Qwen3VL-8B-Instruct			InternVL3.5-1B			
	GF	AUC ↑	AP ↑	FPR ↓	AUC ↑	AP ↑	FPR ↓	AUC ↑	AP ↑	FPR ↓	AUC ↑	AP ↑	FPR ↓
VQA v2 (10k) [22]													
Consist. (Ent)	✗	.624	.471	.925	.677	.266	.896	.684	.423	.891	.535	.249	.956
Consist. (Max)	✗	.620	.470	.914	.678	.266	.896	.680	.421	.891	.535	.249	.956
NLL	✗	.531	.389	.991	.425	.145	.995	.450	.253	.991	.547	.211	.986
Verbalized Conf	✗	.545	.419	.913	.608	.218	.877	.651	.460	.808	.623	.350	.846
P(Correct)	✗	.600	.454	.913	.724	.361	.795	.740	.554	.743	.610	.274	.982
VL Uncertainty	✗	.630	.520	.849	.684	.355	.776	.665	.448	.836	.623	.339	.878
COMET (Ours)	✓	.833	.765	.609	.844	.524	.644	.836	.664	.664	.773	.542	.709
VizWiz (val) [23]													
Consist. (Ent)	✗	.594	.697	.908	.640	.656	.906	.634	.701	.904	.475	.590	.959
Consist. (Max)	✗	.596	.697	.908	.639	.656	.906	.634	.701	.904	.475	.590	.959
NLL	✗	.567	.669	.942	.497	.543	.975	.427	.547	.980	.566	.575	.975
Verbalized Conf	✗	.606	.723	.823	.531	.564	.895	.656	.773	.727	.655	.751	.786
P(Correct)	✗	.756	.827	.786	.718	.734	.839	.715	.796	.734	.734	.772	.839
VL Uncertainty	✗	.662	.767	.837	.641	.687	.842	.658	.761	.806	.679	.746	.854
COMET (Ours)	✓	.783	.849	.732	.793	.813	.696	.815	.865	.663	.752	.813	.759
OK-VQA [24]													
Consist. (Ent)	✗	.655	.611	.921	.666	.471	.895	.653	.520	.918	.477	.393	.963
Consist. (Max)	✗	.654	.610	.921	.663	.470	.895	.652	.519	.918	.477	.393	.963
NLL	✗	.609	.577	.955	.553	.384	.953	.548	.452	.938	.615	.512	.887
Verbalized Conf	✗	.621	.635	.790	.548	.352	.916	.619	.561	.826	.641	.535	.888
P(Correct)	✗	.698	.663	.892	.693	.514	.876	.689	.606	.821	.658	.551	.870
VL Uncertainty	✗	.660	.651	.869	.667	.524	.817	.650	.568	.853	.608	.519	.876
COMET (Ours)	✓	.740	.738	.781	.715	.557	.813	.746	.656	.776	.677	.586	.844

Table E.2: **Unanswerability and hallucination detection results.** Details are the same as Tab. E.1.

Method	Qwen3VL-2B-Instruct			Qwen3VL-4B-Instruct			Qwen3VL-8B-Instruct			InternVL3.5-1B			
	GF	AUC ↑	AP ↑	FPR ↓	AUC ↑	AP ↑	FPR ↓	AUC ↑	AP ↑	FPR ↓	AUC ↑	AP ↑	FPR ↓
VizWiz (unanswerable) [23]													
Consist. (Ent)	✗	.608	.408	.852	.628	.437	.823	.656	.443	.852	.465	.307	.933
Consist. (Max)	✗	.607	.409	.864	.628	.436	.852	.654	.443	.852	.465	.307	.933
NLL	✗	.570	.383	.942	.526	.329	.944	.413	.272	.982	.560	.341	.935
Verbalized Conf	✗	.615	.470	.961	.553	.360	.939	.621	.521	.946	.727	.575	.952
P(Correct)	✗	.751	.576	.712	.660	.421	.764	.600	.397	.839	.788	.594	.628
VL Uncertainty	✗	.651	.450	.910	.545	.367	.957	.543	.359	.950	.693	.481	.860
COMET (Ours)	✓	.788	.596	.641	.767	.556	.641	.797	.635	.689	.808	.641	.628
HallusionBench [25]													
Consist. (Ent)	✗	.564	.631	.920	.569	.439	.932	.572	.442	.920	.522	.575	.919
Consist. (Max)	✗	.562	.630	.920	.567	.431	.957	.566	.438	.920	.521	.574	.919
NLL	✗	.443	.548	.981	.567	.425	.943	.585	.434	.943	.468	.524	.966
Verbalized Conf	✗	.583	.664	.945	.543	.435	.921	.604	.486	.876	.503	.545	.956
P(Correct)	✗	.594	.661	.921	.636	.527	.836	.670	.536	.848	.510	.512	.995
VL Uncertainty	✗	.417	.717	1.000	.500	.393	1.000	.500	.393	1.000	.429	.571	.909
COMET (Ours)	✓	.715	.791	.779	.644	.523	.881	.605	.510	.841	.656	.658	.906

Table E.3: **Multiple Choice Question (MCQ) VQA results.** Details are the same as Tab. E.1. Note that Candidate (Ent) and (Max) use the candidate set information, while the other methods do not.

	Qwen3VL-2B-Instruct			Qwen3VL-4B-Instruct			Qwen3VL-8B-Instruct			InternVL3.5-1B		
	AUC ↑	AP ↑	FPR ↓	AUC ↑	AP ↑	FPR ↓	AUC ↑	AP ↑	FPR ↓	AUC ↑	AP ↑	FPR ↓
MMMU Test[26]												
Candidate (Ent)	✓ .732	.859	.812	.700	.692	.880	.692	.661	.856	.559	.648	.920
Candidate (Max)	✓ .717	.850	.832	.694	.680	.896	.685	.647	.872	.552	.642	.933
Consist. (Ent)	✗ .804	.926	.511	.707	.794	.669	.695	.740	.741	.638	.751	.845
Consist. (Max)	✗ .796	.922	.557	.705	.790	.690	.691	.732	.744	.634	.746	.855
NLL	✗ .155	.575	.997	.271	.431	.995	.337	.432	.977	.386	.539	.990
Verbalized Conf	✗ .666	.832	.934	.521	.621	.950	.552	.586	.923	.521	.654	.940
P(Correct)	✗ .430	.680	.981	.743	.775	.769	.702	.696	.830	.580	.691	.903
VL Uncertainty	✗ .837	.941	.404	.696	.770	.727	.697	.730	.762	.579	.692	.915
COMET (Ours)	✓ .875	.956	.350	.777	.819	.688	.770	.783	.725	.630	.730	.880
MMMU Pro [27]												
Candidate (Ent)	✓ .725	.903	.775	.672	.803	.853	.680	.784	.807	.598	.770	.934
Candidate (Max)	✓ .715	.898	.800	.659	.786	.887	.672	.770	.850	.583	.763	.929
Consist. (Ent)	✗ .769	.928	.612	.696	.847	.670	.708	.831	.695	.662	.814	.884
Consist. (Max)	✗ .757	.921	.635	.694	.845	.700	.705	.826	.700	.648	.801	.916
NLL	✗ .192	.659	.996	.293	.554	.995	.359	.569	.968	.439	.673	.993
Verbalized Conf	✗ .626	.834	.946	.493	.713	.961	.564	.677	.925	.521	.741	.928
P(Correct)	✗ .522	.781	.970	.711	.828	.758	.704	.802	.760	.555	.747	.935
VL Uncertainty	✗ .815	.949	.448	.703	.839	.730	.714	.825	.709	.652	.810	.873
COMET (Ours)	✓ .834	.953	.442	.739	.851	.778	.726	.811	.794	.610	.771	.931
MMStar [28]												
Candidate (Ent)	✓ .701	.643	.810	.669	.533	.849	.654	.492	.874	.590	.554	.909
Candidate (Max)	✓ .692	.632	.803	.667	.524	.858	.651	.489	.879	.592	.548	.921
Consist. (Ent)	✗ .753	.844	.564	.723	.797	.574	.740	.800	.539	.741	.848	.574
Consist. (Max)	✗ .746	.837	.567	.719	.786	.644	.732	.785	.622	.739	.847	.574
NLL	✗ .226	.434	.995	.177	.352	.999	.206	.356	.996	.247	.462	.999
Verbalized Conf	✗ .559	.651	.919	.607	.694	.821	.564	.658	.850	.551	.691	.808
P(Correct)	✗ .581	.604	.958	.732	.725	.763	.793	.815	.581	.634	.710	.896
VL Uncertainty	✗ .754	.838	.593	.765	.827	.524	.754	.811	.590	.529	.644	.917
COMET (Ours)	✓ .819	.878	.523	.830	.859	.501	.853	.881	.444	.739	.815	.743

Table E.4: **Impact of λ** . We use Qwen3VL-8B-Instruct as the backbone. Hyperparameters are selected on the MMMU validation split (the first column).

λ	MMMU val	VQA v2	VizWiz (val)	OK-VQA	MMMU Test	MMMU Pro	MMStar	Average
0	.837	.834	.734	.735	.753	.707	.857	.780
0.25	.842	.836	.815	.746	.770	.726	.853	.798
0.5	.822	.841	.796	.741	.772	.715	.835	.789
1	.828	.839	.821	.751	.767	.707	.852	.795

Table E.5: **Impact of β, γ** . Details are the same as Tab. E.4.

β/γ	MMMU val	VQA v2	VizWiz (val)	OK-VQA	MMMU Test	MMMU Pro	MMStar	Average
0.2/-0.1	.842	.836	.815	.746	.770	.726	.853	.798
1/0	.835	.837	.796	.746	.760	.736	.832	.792

E.3 Runtime analysis

Our method does not require additional generation. However, the multimodal understanding benchmarks used in our experiments are usually sufficient with very short generated tokens (*e.g.*, “A” for MCQ VQA tasks or “A cat” for open-ended VQA tasks). Therefore, we set the maximum generated tokens to 4,096 to examine the scenario when we need to generate a longer-context output; this could include the reasoning trace [55], or long context generation.

Tab. E.6 shows the results. We randomly select 100 samples from the VQA v2 dataset and measure the runtime for uncertainty estimation methods. In this experiment, CoMET shows the most efficient inference time uncertainty estimation. Specifically, compared to sampling-based methods, such as consistency (we generate five diverse samples) and VL Uncertainty (we randomly generate five noises), CoMET performs much faster inference, but achieves significantly better uncertainty estimation performance as shown in the main results.

For training, we use one L40 GPU for each training, while training takes about 3-6 hours with the selected hyperparameters and our collected dataset (after cache extraction). For evaluation, consistency or VL uncertainty take more than a day with 1 L40 GPU when we have approximately 10k samples (*e.g.*, VQA v2, MMMU test); meanwhile, because CoMET can re-use the cached features, once features are cached, it takes less than a minute to evaluate; cache extraction takes about 3-4 hours in the same setting.

E.4 Impact of adaptation

Tab. E.7 shows the impact of our lightweight adaptation method. Even without adaptation, CoMET already provides a meaningful uncertainty signal compared to strong baselines, such as Verbalized confidence and P(Correct) (average AUROC 0.609 vs. 0.604 and 0.598, respectively). By adapting CoMET on the MMMU validation split, CoMET ties with VL uncertainty, the strongest baseline in average AUROC. By adding VQA samples for the adaptation, the uncertainty estimation by CoMET is significantly improved.

Importantly, the effect depends on the adaptation source. MMMU-only adaptation specializes the uncertainty head to MCQ evaluation (MMMU, MMMU-Pro, and MMStar), while open-ended VQA performances are somewhat worse than the original (*e.g.*, OK-VQA AUROC 0.621 \rightarrow 0.593 after the MMMU-only adaptation). In contrast, VQA-only adaptation significantly improves open-ended VQA tasks, but its MCQ performance is somewhat worse than that of the MMMU-only adaptation. Combining VQA and MMMU adaptation gives the best average performance, suggesting that the two sources provide complementary calibration signals.

Table E.6: **Runtime Analysis**. We report the average throughput of uncertainty estimation methods on the sampled VQA v2 dataset using the Qwen3VL-2B-Instruct model with CoMET. The number of maximum generation tokens is set to 4096 in this experiment. Runtime is measured on a single RTX 3090 GPU.

Methods	Throughput (s)
Consistency	34.87
NLL	5.95
Verbalized Conf	6.10
P(Correct)	6.01
VL Uncertainty	16.33
CoMET (Ours)	5.88

Table E.7: **Impact of the adaptation strategy.** Measured by the Qwen3VL-8B-Instruct backbone.

Method	VQA v2	VizWiz	OK-VQA	MMM U Test	MMM U Pro	MMStar	Avg
COMET (No Adapt)	.503	.676	.621	.671	.659	.526	.609
COMET (MMM U only adapt)	.654	.730	.593	.772	.731	.863	.724
COMET (VQA only adapt)	.826	.816	.726	.702	.678	.804	.759
COMET (VQA + MMM U adapt)	.836	.815	.746	.770	.726	.853	.791
Consist (ent)	.624	.594	.655	.732	.725	.701	.672
Verbalized Confidence	.545	.606	.621	.666	.626	.559	.604
P(Correct)	.600	.756	.698	.430	.522	.581	.598
VL uncertainty	.630	.662	.660	.837	.815	.754	.726

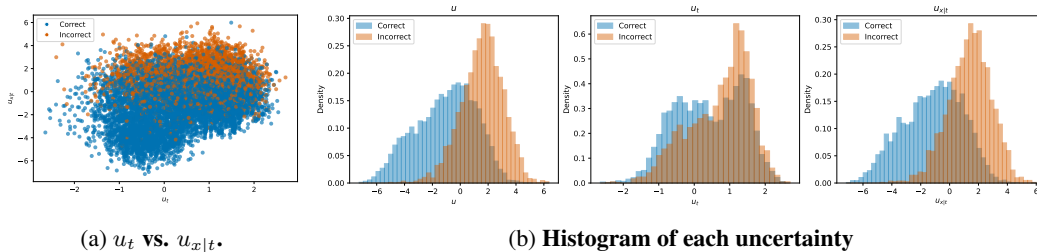


Figure E.1: **Statistics of uncertainty values.** We plot the statistics related to u , u_t , and $u_{x|t}$ on the VQA v2 dataset using the Qwen3VL-2B-Instruct model. Blue samples denote correct samples, while orange samples denote incorrect samples.

E.5 Visualization

Fig. E.1 shows the statistics of uncertainties on VQA v2 datasets using the Qwen3VL-2B-Instruct model. Blue and orange samples correspond to correct and incorrect samples, respectively.

For the qualitative visualizations, we use COMET with the Qwen3VL-8B-Instruct model. We visualize the samples having high and low uncertainty in each uncertainty term: Fig. E.2 shows the samples with our proposed uncertainty, Fig. E.3 shows the samples with context-specific uncertainty u_t , and Fig. E.4 shows the samples with multiplicity-specific uncertainty $u_{x|t}$.

In addition, we illustrate the samples having the same x but different t in Fig. E.5. As shown in the figure, the level of uncertainty can be changed a lot by choosing different context. For example, “Is this food ready to eat” can be answered easily, but “Is this pizza homemade?” is somewhat hard to answer; we need more information to answer the question.

We also visualize the samples having the same context (question) t but different input (image x) in Fig. E.6. Even with the same t (therefore, having the same u_t), the degree of uncertainty could vary a lot as shown in the figure.

Finally, we report the samples with opposing u_t and $u_{x|t}$, *e.g.*, u_t is high but $u_{x|t}$ is low, and vice versa. Fig. E.7 shows the samples. For example, even though a question can be answered in just two answers (“yes” or “no”; so u_t is very low), it is somewhat difficult to answer the question “Are all people about the same age?” in the first example, resulting in a high uncertainty value due to $u_{x|t}$.

F Discussion and Limitation

Limitation in theory. In theory, we use two assumptions: Fig. 2 and the uniform assumption on $p(y | t)$. Although we believe that they are reasonable and not strong assumptions, these do not generalize to case where Fig. 2 does not hold or where $p(y | t)$ is not a uniform distribution. However, our assumption can be viewed as a relaxed version of those cases; furthermore, the empirical evidence supports that our formulation is suitable in many scenarios, including multimodal understanding, error detection, and multimodal MCQ tasks.

Limitation in method design. Although our formulation is model-agnostic and can be generalized to any form of multimodal tasks, our actual method design has some limitations.

The first limitation of COMET in terms of method design is the approximation of $p(y | t)$, or specifically K_t . However, we believe that the approximation is one of the most reasonable and sound ways considering that the true $p(y | t)$ is impossible to access. We also use a control parameter λ to control the approximation error induced by this approximation; our experiments show that $\lambda = 1$ (*i.e.*, using the approximation without any control) actually performs well on average (Tab. E.4); we chose $\lambda = 0.25$ because it performs the best in the hyperparameter selection criteria (*i.e.*, MMMU validation), but in practice, we believe that $\lambda = 1$ is also acceptable, considering the empirical evidence in our parameter study.

Another limitation is the quality of the matching probability module, *i.e.*, MLLM-as-verifier. As shown in Fig. C.2, the MLLM-as-verifier is not a perfect estimator; the quality of matching probability estimator can degrade the performance of COMET as shown in Appendix C.1. This makes the framework simple and broadly applicable, but the resulting uncertainty targets can inherit calibration errors or semantic biases from the verifier. We partially address this issue through validation-based calibration, but a more principled calibration of semantic matching probabilities remains an interesting direction for future work.

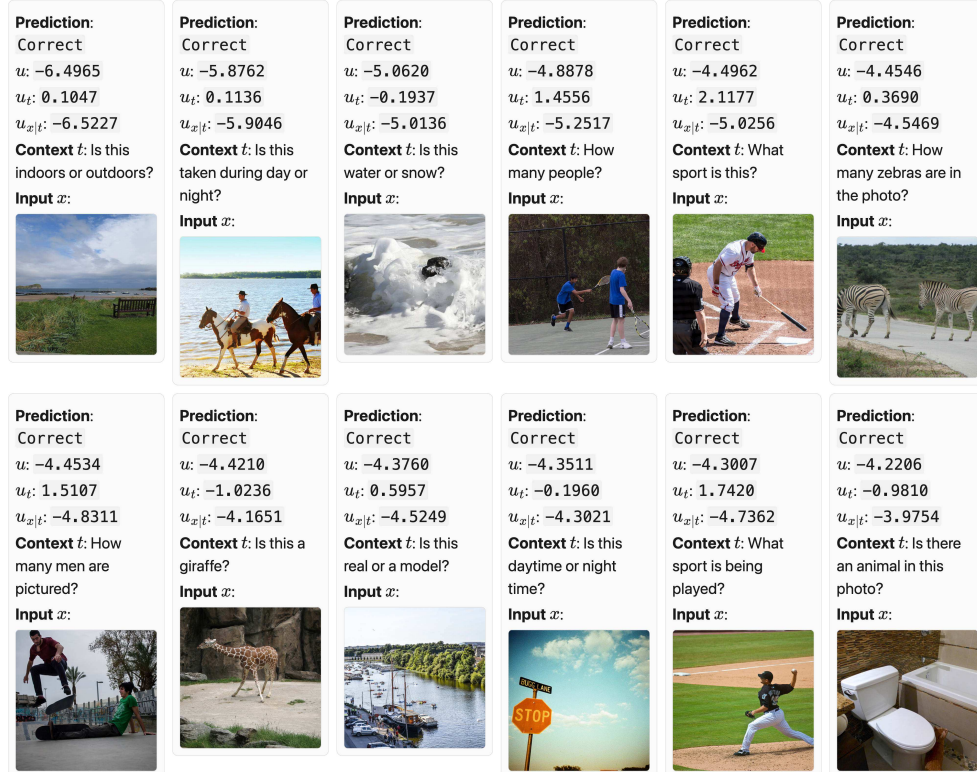
Potential extensions. Although this paper focuses on open-ended multimodal VQA, the proposed formulation is not limited to this setting. More broadly, X can denote an observed input, T can denote the task context or environment specification that constrains the valid outputs, and Y can denote a candidate response or action. For example, in agentic AI settings, uncertainty may arise from ambiguity in the user request, the environment state, or the set of valid actions [56]. In this case, X can denote the observed state or user input, T can denote the task context or environment specification, and Y can denote a candidate response or action. Similarly, for reasoning models, the context t can include an intermediate reasoning trace that define the space of acceptable outputs. We leave a systematic study of these broader settings to future work.

G Broader impacts

This work aims to provide a better multimodal predictive uncertainty of MLLMs, which potentially supports safer deployment in high-stakes scenarios. We do not anticipate direct negative impacts specific to COMET beyond those of uncertainty-aware MLLMs in general.

Final uncertainty u

Most certain



Most uncertain

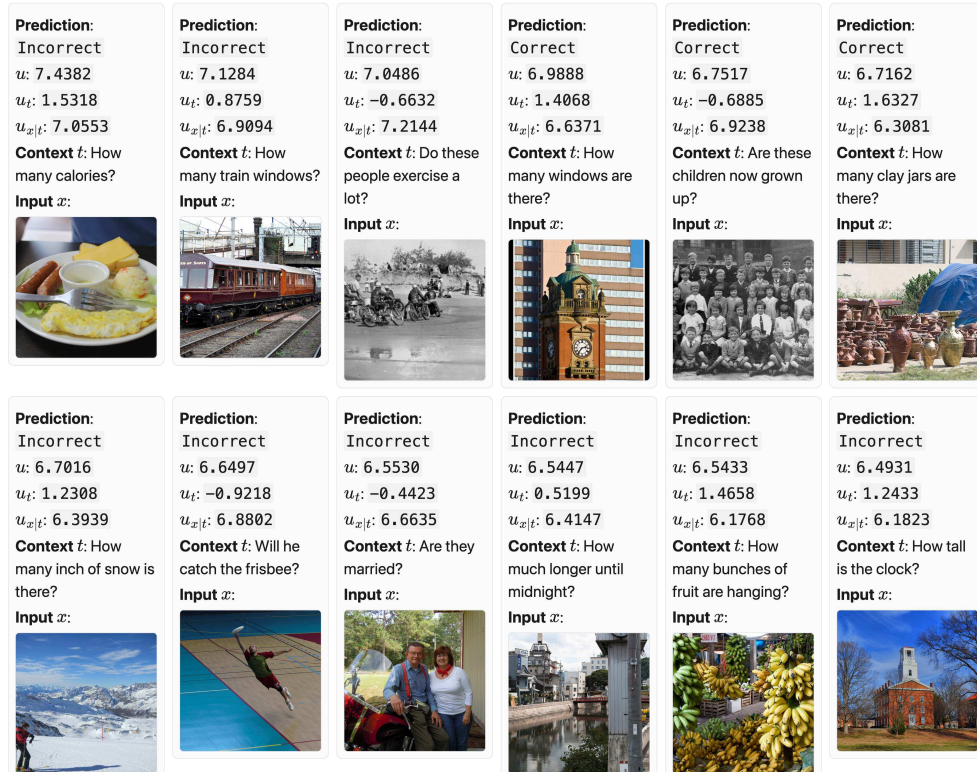
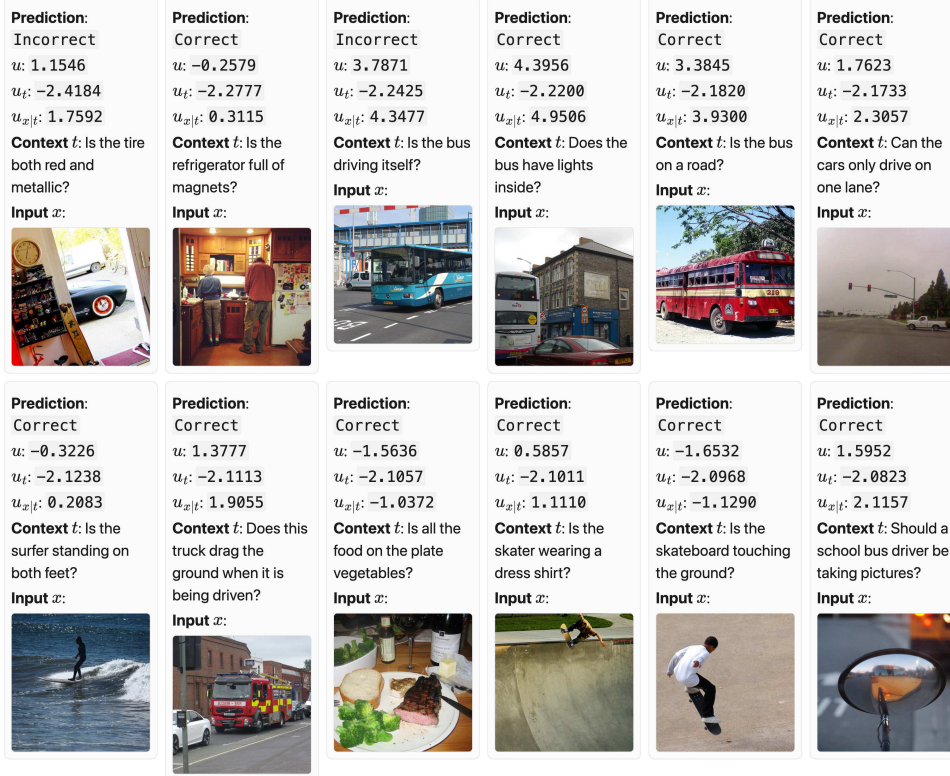


Figure E.2: Visualization of the certain/uncertain samples by the proposed uncertainty scores u .

Task uncertainty u_t

Most certain



Most uncertain

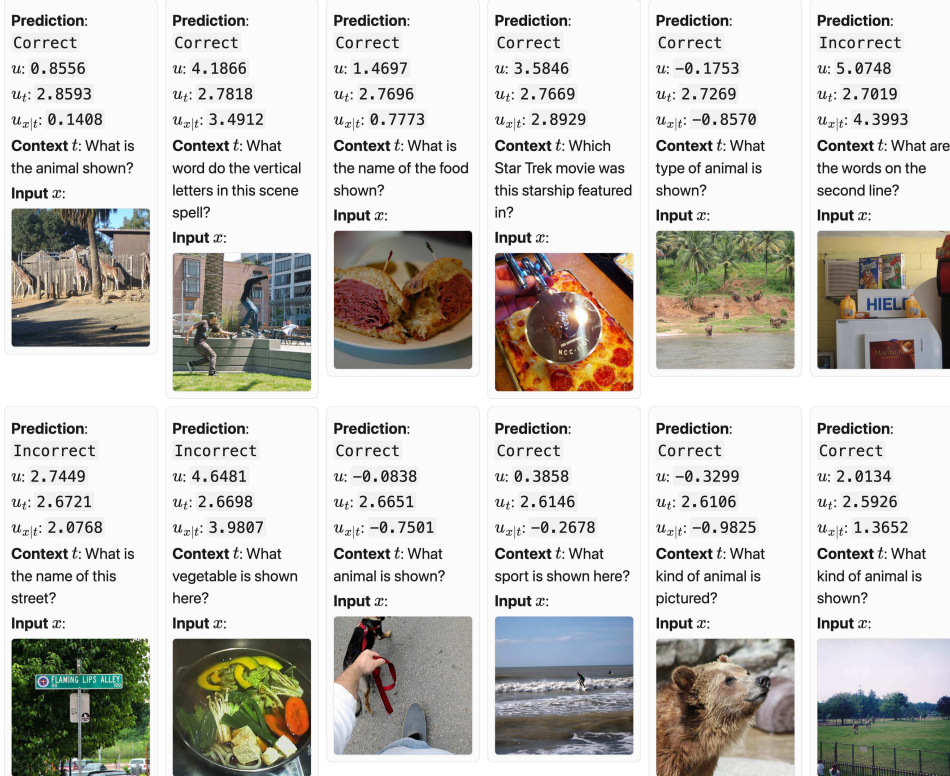
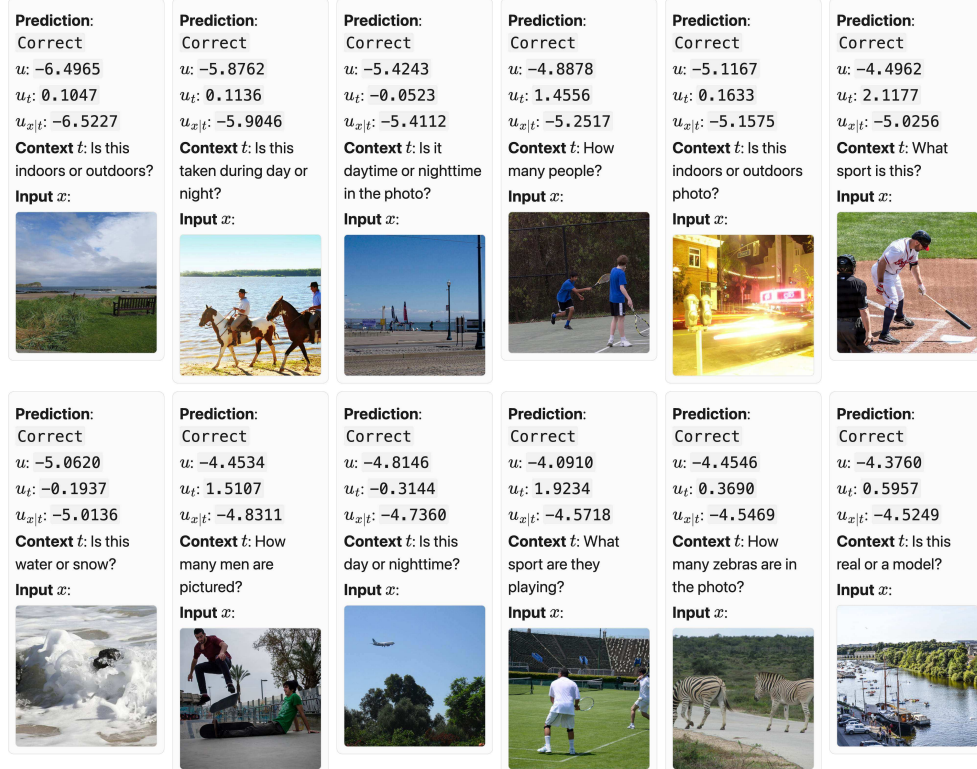


Figure E.3: Visualization of the certain/uncertain samples by the context-specific uncertainty scores u_t .

Image-conditioned uncertainty $u_{x,t}$

Most certain



Most uncertain



Figure E.4: Visualization of the certain/uncertain samples by the multiplicity-specific uncertainty scores $u_{x|t}$.

Same Image, Different Questions by u




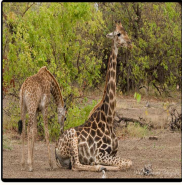



	Prediction	u	u_t	$u_{x t}$	Context t
	Correct	-5.4243	-0.0523	-5.4112	Is it daytime or nighttime in the photo?
	Incorrect	4.7103	-1.5009	5.0856	Is it summer?
	Prediction	u	u_t	$u_{x t}$	Context t
	Correct	-3.8697	0.3690	-3.9619	How many zebras are in the photo?
	Incorrect	4.9631	0.6115	4.8102	How many stripes on the zebra on the right?
	Prediction	u	u_t	$u_{x t}$	Context t
	Correct	-2.5025	-1.3541	-2.1640	Is the man skateboarding?
	Incorrect	5.8100	1.2954	5.4861	How tall is the wave in this picture?
	Prediction	u	u_t	$u_{x t}$	Context t
	Correct	-2.7855	1.8233	-3.2413	How many animals?
	Correct	-0.7946	-1.6813	-0.3743	Is the giraffe behind a fence?
	Incorrect	0.5428	-0.9541	0.7813	Is this giraffe at the zoo?
	Incorrect	5.0513	-0.5124	5.1794	How tall is the giraffe?
	Prediction	u	u_t	$u_{x t}$	Context t
	Correct	-2.8732	-1.0869	-2.6015	Is this a pickup truck?
	Incorrect	4.5726	1.3015	4.2472	What company made the white car?
	Prediction	u	u_t	$u_{x t}$	Context t
	Correct	-2.4693	-1.3881	-2.1223	Is the food ready to eat?
	Correct	1.3160	-0.5751	1.4597	Is this a special plate for this type of dessert?
	Incorrect	4.8152	-1.3319	5.1481	Is this pizza homemade?
	Prediction	u	u_t	$u_{x t}$	Context t
	Correct	-1.4730	0.5779	-1.6175	How many busses can be seen?
	Incorrect	4.8565	-0.9150	5.0853	Is it cold out?
	Incorrect	5.7690	1.3067	5.4423	What number of seats are on the bus?

Figure E.5: Uncertainty can vary by context t even with the same input x .

Same Question, Different Images by u

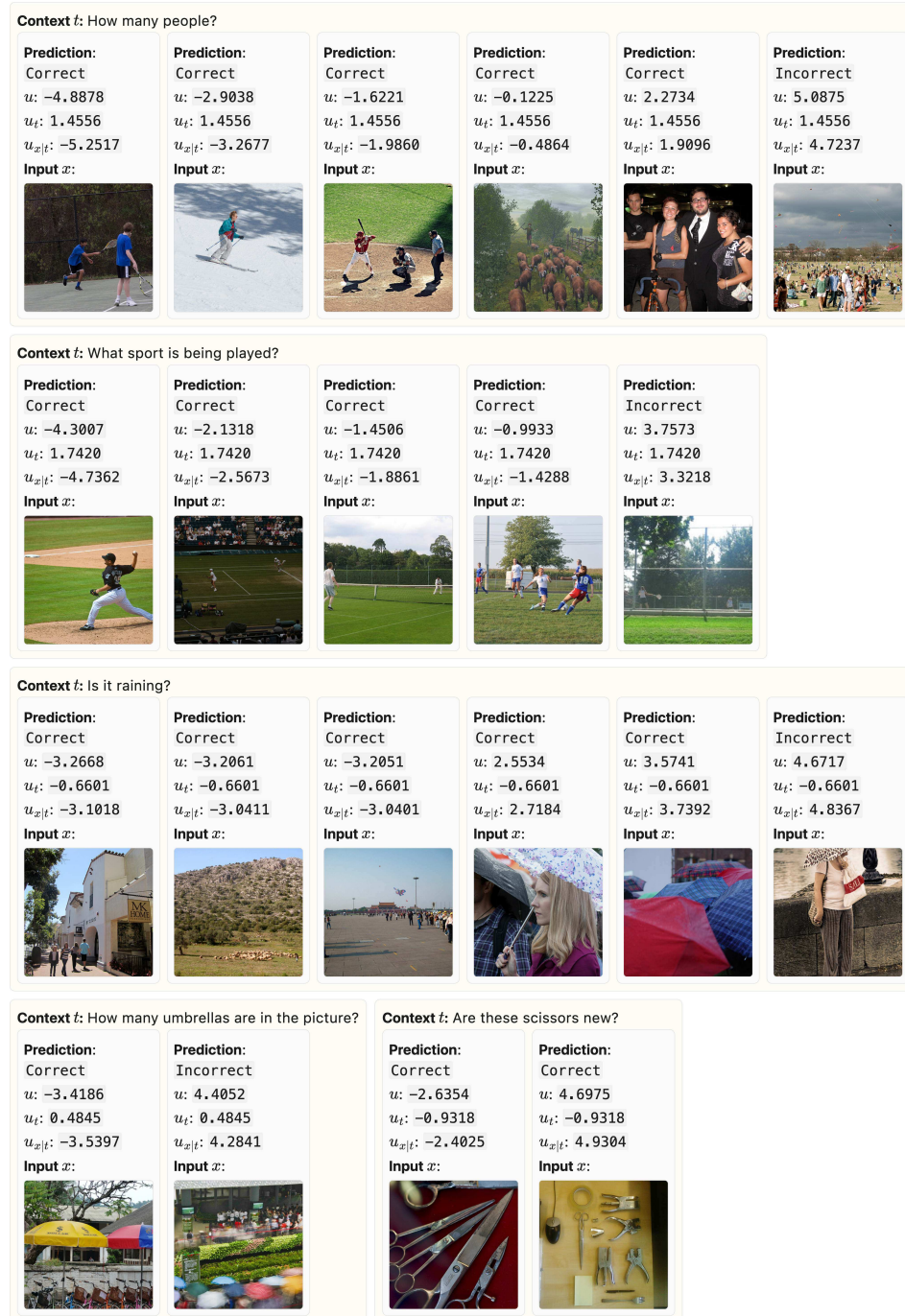














Figure E.6: Uncertainty can vary by the relationship between $x | t$ and the set of plausible answers y (i.e., their multiplicity), even with the same input t .

Low u_t , High $u_{x|t}$

<p>Prediction: Incorrect u: 5.2004 u_t: -1.8609 $u_{x t}$: 5.6656 Context t: Are all people about the same age?</p> 	<p>Prediction: Incorrect u: 4.8970 u_t: -1.7974 $u_{x t}$: 5.3464 Context t: Would these personal motorized vehicles likely belong to a biker gang?</p> 	<p>Prediction: Correct u: 4.8262 u_t: -1.7712 $u_{x t}$: 5.2690 Context t: Are all of the elephants adults?</p> 	<p>Prediction: Correct u: 4.3956 u_t: -2.2200 $u_{x t}$: 4.9506 Context t: Does the bus have lights inside?</p> 	<p>Prediction: Correct u: 4.7082 u_t: -1.6135 $u_{x t}$: 5.1115 Context t: Has this kitchen most likely been cleaned recently?</p> 	<p>Prediction: Incorrect u: 5.1363 u_t: -1.5437 $u_{x t}$: 5.5222 Context t: Will the train travel through the forest?</p> 
<p>Prediction: Incorrect u: 4.8175 u_t: -1.5317 $u_{x t}$: 5.2004 Context t: Is the zebra shy?</p> 	<p>Prediction: Correct u: 4.3108 u_t: -1.7917 $u_{x t}$: 4.7587 Context t: Can the plane carry more than 100 people?</p> 	<p>Prediction: Incorrect u: 5.3304 u_t: -1.5080 $u_{x t}$: 5.7074 Context t: Is this a beginner's class?</p> 	<p>Prediction: Incorrect u: 4.8828 u_t: -1.4923 $u_{x t}$: 5.2559 Context t: Is the surfer enjoying his activity?</p> 	<p>Prediction: Incorrect u: 6.0135 u_t: -1.4839 $u_{x t}$: 6.3844 Context t: Is the man giving a speech?</p> 	<p>Prediction: Incorrect u: 4.3391 u_t: -1.4768 $u_{x t}$: 4.7083 Context t: Does the cat look thirsty?</p> 

High u_t , Low $u_{x|t}$



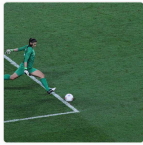


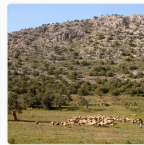
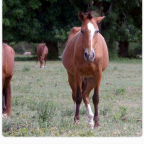


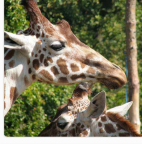


<p>Prediction: Correct u: -2.6972 u_t: 2.5293 $u_{x t}$: -3.3296 Context t: What game is this?</p> 	<p>Prediction: Correct u: -2.9707 u_t: 2.4295 $u_{x t}$: -3.5781 Context t: What game is this?</p> 	<p>Prediction: Correct u: -2.1097 u_t: 2.4295 $u_{x t}$: -2.7170 Context t: What game is this?</p> 	<p>Prediction: Correct u: -1.8226 u_t: 2.4295 $u_{x t}$: -2.4300 Context t: What game is this?</p> 	<p>Prediction: Correct u: -1.6436 u_t: 2.2539 $u_{x t}$: -2.2071 Context t: What flower is this?</p> 	<p>Prediction: Correct u: -0.8913 u_t: 2.2147 $u_{x t}$: -1.4449 Context t: What type of animal are these?</p> 
<p>Prediction: Correct u: -3.1121 u_t: 2.2112 $u_{x t}$: -3.6649 Context t: What animals are these?</p> 	<p>Prediction: Correct u: -1.6740 u_t: 2.1999 $u_{x t}$: -2.2240 Context t: What type of animal is this?</p> 	<p>Prediction: Correct u: -1.0459 u_t: 2.1999 $u_{x t}$: -1.5959 Context t: What type of animal is this?</p> 	<p>Prediction: Correct u: -1.1769 u_t: 2.1859 $u_{x t}$: -1.7234 Context t: What are these animals?</p> 	<p>Prediction: Correct u: -0.7522 u_t: 2.2914 $u_{x t}$: -1.3250 Context t: What is this food?</p> 	<p>Prediction: Correct u: -1.9259 u_t: 2.1529 $u_{x t}$: -2.4641 Context t: Where in the world is this?</p> 

Figure E.7: Samples with opposing uncertainty components. Top: low u_t and high $u_{x|t}$. Bottom: high u_t and low $u_{x|t}$. These examples illustrate cases where task-only and image-conditioned uncertainty provide conflicting signals.